Composite Structures 256 (2021) 113097

Contents lists available at ScienceDirect

Composite Structures

journal homepage: www.elsevier.com/locate/compstruct

Isogeometric static analysis of laminated plates with curvilinear fibers based on Refined Zigzag Theory

K.A. Hasim [a,*], A. Kefal [b,c,d]

[a] Department of Civil Engineering, Adana Alparslan Turkes Science and Technology University, Adana 01250, Turkey
[b] Faculty of Engineering and Natural Sciences, Sabanci University, Tuzla, Istanbul 34956, Turkey
[c] Integrated Manufacturing Technologies Research and Application Center, Sabanci University, Tuzla, Istanbul 34956, Turkey
[d] Composite Technologies Center of Excellence, Istanbul Technology Development Zone, Sabanci University-Kordsa, Pendik, Istanbul 34906, Turkey

ARTICLE INFO

Keywords:
Composite
Curvilinear
Zigzag functions
Isogeometric
Finite element
Single-layer theory

ABSTRACT

In this study, we propose a new IsoGeometric formulation based on Refined Zigzag Theory (RZT), abbreviated as IG-RZT, for static analysis of laminated plates and sandwich panels with curvilinear fiber paths for the first time in literature. The original RZT formulation defines constant, linear, and zigzag deformation contributions of thickness coordinate to the in-plane displacements. This kinematic relation can accurately predict in-plane displacement of composite with straight fibers. However, estimating a realistic variation of in-plane displacements in a variable angle tow (VAT) composite is a more challenging problem as compared to the straight fiber composites. This difficulty has been addressed herein by including a quartic (fourth-order) polynomial thickness expansion that includes the transverse normal strain effects to the kinematic displacement fields of RZT. Moreover, the modelling of VAT composites results in the RZT zigzag functions to depend not only on the thickness coordinate but also on the in-plane positions. The present IG-RZT methodology is free of shear-locking and shear correction factors due to the integration of RZT with Non-Uniform Rational B-Splines (NURBS) functions of isogeometric analysis. The use of NURBS functions also enable the exact geometry data to be taken directly from a computer aided design (CAD) software, e.g., Rhinoceros, into an in-house Mathematica code. The accuracy and efficiency of the present IG-RZT formulation is assessed and validated by solving various examples of curvilinear fiber laminated plates with different aspect and span-to-thickness ratios. Comparison of IG-RZT results with reference solutions available in literature and generated by a commercial software (ANSYS) using 3D finite elements have demonstrated the remarkable benefits of the proposed IG-RZT method for predicting highly accurate both displacement and stress distributions of VAT composite structures.

1. Introduction

Since the past decades, studies in aerospace, automotive and marine structures have been constantly seeking answers to the question of how one can produce composite materials that have higher strength and stiffness but require less weight and cost. Until recently, in traditional composite structures, these targets were tried to be achieved by uniform lamination (straight and unidirectional fibers) over the whole structure (Constant Stiffness Composite Laminates-CSCL), and it was focused on increasing the number and thickness of the layers or changing the uniform fiber angle in the layer. However, due to their low transverse shear modulus, laminated composites can exhibit significant transverse shear deformation than the isotropic counterparts and thus, when designing composite structures, it is also important to obtain the accurate strain and stress fields through the thickness in order to prevent delamination caused by the transverse shear deformations.

Within the context of composite modelling, the theories for the stress–strain analysis of laminated composites can be grouped into two: Layerwise (LW) and Equivalent Single Layer (ESL) theories. In the LW theory [1–6], the thickness coordinate is split into a number of analysis layers and the kinematic displacement fields of each analysis layer have been independently described which makes the theory computationally expensive and dependent on the number of layers considered. The ESL theories [7–11] treat a heterogeneous laminated plate as a statically equivalent, single layer having a complex constitutive behavior, thereby reducing the 3-D continuum problem into 2-D space.

* Corresponding author.
E-mail address: kahasim@atu.edu.tr (K.A. Hasim).

https://doi.org/10.1016/j.compstruct.2020.113097
Received 3 July 2020; Revised 8 September 2020; Accepted 3 October 2020
Available online 8 October 2020
0263-8223/© 2020 Elsevier Ltd. All rights reserved.

Refined Zigzag Theory (RZT), developed by Tessler et al. [12–15], can be counted as one of the ESL theories which accounts for the zigzag pattern of the axial displacements by introducing a zigzag function for each layer. The kinematic variables of the theory are independent from the number of layers which make RZT computationally more efficient. In addition, anomalies for the clamped supports, encountered in the zigzag theory of Averill et al. [16–18] has been corrected in the RZT. Moreover, Gherlone [19] has compared the performances of RZT with Murakami's one [11] and concluded that zigzag functions of RZT lead to more accurate results, especially for arbitrary stacking sequences, and superior even for the case where the external layers of a laminate are weaker than the adjacent layers. Iurlaro et al. [20] have investigated the efficiency of RZT in predicting the static response, natural frequencies and bucking loads of sandwich plates. Barut et al. [21] have proposed a new C^0-continuous triangular plate element based on RZT that considers the transverse normal strain for laminated composite and sandwich plates. The isogeometric static analysis of straight fiber laminated beams and plates using RZT have recently been introduced [22–24]. By using anisoparametric interpolation strategy, Versino et al. [25] have developed a six and three node, C^0-continuous, RZT based triangular plate/shell elements. Ascione and Gherlone [26] have developed a nonlinear formulation of RZT using Von-Karman strain–displacement relations. These studies overall focus on the structural mechanics of composites and sandwich structures with straight fibers.

Later on, the aforementioned studies for the straight fiber laminates were followed by the studies on the Variable Stiffness Composite Laminates (VSCL). The VSCL is based on the idea of changing the lamina stiffness locally which can be enforced by either changing the fiber volume ratio [27] or terminating the inner layers (ply drop-off) to reduce the composite thickness in certain regions [28]. However, the last option can result in highly stress-concentrated regions. With the invention of automated fiber replacement machines, the fibers are not constrained along a straight path, anymore and the concept of variable angle tow composites (VAT) along a curvilinear path enable a further characteristic tailor and improve the structural performance and enhanced capability of laminated composite structures by changing stiffness in the desired areas. Vibrational resonance in aerospace and naval structures can be avoided by designing the laminated plates according to maximum fundamental frequency. Abdalla et al. [29] have shown that the utilization of curvilinear fibers enable laminated composites to attain a higher natural frequency thereby eliminating the potential occurrence of vibrational resonance as compared to the straight fiber composites. Hyer and Lee [30] have explored the benefits of using curvilinear fibers to increase the buckling performance. It was shown that curvilinear fibers of a simply supported plate with a centrally located hole divert the load from the unsupported hole region to the supported edges, thus increasing the buckling capacity. When it is necessary to leave holes or notches in the laminated composite plate, it is clear that these gaps disrupt the continuity of the fiber and adversely affect the load carrying capacity in case of using straight fibers. For this reason, many researchers [31,32] have examined how much the load carrying capacity can be increased by laying curvilinear fibers on the principal tensile and compressive trajectories that appear in accordance with the gap in their experiments. Thus, the load transfer can be carried over the curvilinear fibers instead of resin. Various studies have been conducted to facilitate the placement of curvilinear tows from the manufacturing point of view [33–35]. In addition, the optimization of variable stiffness composites by maximizing its mechanical strength have been studied in a great detail to determine optimal fiber angles throughout the composite structure. Also, these optimization studies aim to satisfy volume/mass and manufacturing (fiber path continuity) constraints [29,36–39] for lean production.

For the structural analysis of curvilinear fiber laminated composites, various numerical methods such as finite element, boundary element, smoothed finite element, mesh-free, differential quadrature etc. [40–47] can be applied in the case of insufficient analytical solutions. Among these numerical approaches, finite element method (FEM) is a well-known one and frequently used in computer aided engineering industry (CAE). The FEM mainly utilizes Lagrangian (C^0 inter-element continuity) or Hermitian (C^1 inter-element continuity) type approximation functions to discretize the unknown kinematic variables of the finite element. However, high degree polynomials used in Lagrangian elements can be unstable and insufficient for the exact definition of complex geometries. In addition, the computer-aided design (CAD) and manufacturing (CAM) industries utilize Non-Uniform Rational B-Splines (NURBS) [48] instead of the former functions to parametrize the geometry, thereby introducing an engineering gap between the two industries, i.e., CAD and CAE.

Fortunately, Hughes et al. [49] introduced a state-of-the-art methodology known as Isogeometric Analysis (IGA), which use the same NURBS basis functions to discretize the geometry and displacement fields. In this regard, requirements for a smoother design geometry, highly precise analysis, and CAD/CAE integrity can be fulfilled without any difficulty. The mathematical backgrounds of NURBS and IGA can be found in the fundamental books of Piegl and Tiller [48] and Cottrell et al. [50], respectively. Albeit to a large collection of IGA studies on composite structures, we only focus on recently published studies for conciseness. For instance, Liu and Jeffers [51] have developed an isogeometric layerwise model for the analysis of straight fiber laminated composite and sandwich plates embedding a functionally graded material core. Thai et al. [52] have developed a generalized shear deformation theory based on IGA by imposing inverse trigonometric functions for the in-plane displacements of the functionally graded isotropic and sandwich plates. Besides, Nguyen et al. [53] have proposed a formulation based on IGA and FSDT for postbuckling analysis of functionally graded carbon nanotube-reinforced composite shells. More recently, Shi et al. [54] have introduced a new hyperbolic tangent higher order shear deformation theory assessed with the NURBS based IGA for the static, free vibration and buckling analysis of laminated composite plates. Nguyen et al. [55] have proposed a novel, generalized three-variable shear deformation plate theory by using the high-order continuity advantage of IGA. Recently, Nguyen et al. [56] have studied on the analysis of free vibration, buckling and instability of functionally graded porous plates, reinforced by graphene platelets using three-variable shear deformation theory. Furthermore, Fantuzzi and Tornabene [57] have employed strong form finite elements with isogeometric mapping for arbitrarily shaped laminated composite plates. With the development of micro electromechanical systems, recent studies are dedicated to investigating the small-scale effects for the bending, buckling and thermal analyses of layered composite microplates utilizing isogeometric analysis [58,59].

Most of the IGA studies regarding composite structures are mainly dedicated to the structural analysis of straight fiber laminated beams/-plates/shells. To the best of authors' knowledge, there is currently no study available in literature concerning IGA of laminated plates with curvilinear paths that provides a rigorous mathematical formulation based on RZT. In this study, we propose a novel structural analysis methodology based on the coupling of isogeometric framework and RZT for accurately modelling VAT composite and sandwich structures. We envisage that the present IG-RZT formulation can address the shortcomings of finite element-based techniques available in literature, especially in the case of predicting accurate through-the-thickness distributions of stresses and strains with less computational cost.

This study is organized as follows. In the first part of IG-RZT mathematical formulation, the original form of RZT displacement fields is extended into higher order thickness expansions. In Section 3, the foundations of NURBS functions and IGA are briefly discussed. On the basis of these formulations, we provide the coupling of IGA and

RZT for VAT composite structures in Section 4. In Section 5, numerical results are obtained for the bending of square and circular laminated composite plates and sandwich structures with curvilinear paths. The results are compared with high-fidelity 3-D ANSYS models and other reference solutions taken from the literature. The final section is devoted to the main conclusions that may be drawn from the present numerical results.

2. Fundamentals of RZT

As depicted in Fig. 1, a reference coordinate system $(x,y,z)\equiv(\boldsymbol{x},z)$ with its origin $(0,0,0)$ is located on the mid-plane of the laminated plate with curvilinear fibers to describe the positive directions of the kinematic variables of the present study. The laminate has N layers with a uniform thickness of $2\,h$, length of a and width of b. Recently, Tessler et al. [12–14,60] have developed a robust refined zigzag theory (RZT) that the zigzag functions, $\phi_i^{(k)}$ are piecewise linear through the thickness and satisfies all the boundary conditions to be modelled correctly. For brevity of the study, we report herein only the essential knowledge of RZT and the reader can find further details in various studies of [12–14,60].

According to the original RZT formulation [60], the zigzag functions for the k-th ply of a given laminate can be defined as:

$$\phi_i^{(k)}=\tfrac{1}{2}\left(1-\xi^{(k)}\right)\bar{u}_i^{(k-1)}+\tfrac{1}{2}\left(1+\xi^{(k)}\right)\bar{u}_i^{(k)};\quad (i=1,2) \tag{1a}$$

$$\xi^{(k)}=\frac{z-\left(z_k+h^{(k)}\right)}{h^{(k)}};\left(z_1=-h,\qquad z_k=z_{k-1}+2h^{(k)}\right) \tag{1b}$$

where the $\xi^{(k)}\in[-1,1]$ and $\bar{u}_i^{(k)}$ terms represent the layer thickness coordinate and the interfacial axial displacements, respectively. Here, the mathematical construction of the zigzag functions leads to identically vanishing the interfacial axial displacements at the bounding surfaces of the laminate, $\bar{u}_i^{(0)}=\bar{u}_i^{(N)}=0$. On the other hand, these layerwise displacements can be calculated recursively as [12–14,60]:

$$\bar{u}_i^{(k)}=2h^{(k)}\beta_i^{(k)}+\bar{u}_i^{(k-1)} \tag{2}$$

with the slope of the zigzag functions, $\beta_i^{(k)}$ which is defined as:

$$\beta_i^{(k)}=\frac{h\left(\sum_{k=1}^{N_L}\frac{h^{(k)}}{\hat{G}_{iz}^{(k)}}\right)^{-1}}{\hat{G}_{iz}^{(k)}}-1;\quad (i=1,\ 2) \tag{3}$$

where the $\hat{G}_{1z}^{(k)};\hat{G}_{2z}^{(k)}$ parameters stand for the global transverse-shear moduli of the laminae through the x and y directions, respectively.

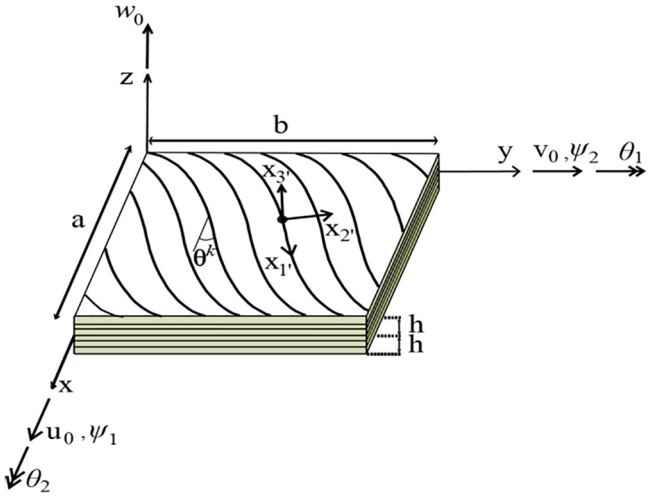

Fig. 1. Rectangular laminated geometry with a curvilinear path.

For a composite lamina composed of straight fibers, these terms are constant over the in-plane coordinates of plate, $\boldsymbol{x}\equiv(x,y)$. However, they naturally become functions of the x and y in case of modelling a tow-steered fiber reinforced composites which can be mathematically proved by the transformation below as:

$$\begin{Bmatrix}\hat{G}_{1z}^{(k)}(\boldsymbol{x})\\ \hat{G}_{2z}^{(k)}(\boldsymbol{x})\end{Bmatrix}=\begin{Bmatrix}G_{1'z}^{(k)}\mathrm{Cos}^2\theta^{(k)}(\boldsymbol{x})+G_{2'z}^{(k)}\mathrm{Sin}^2\theta^{(k)}(\boldsymbol{x})\\ G_{2'z}^{(k)}\mathrm{Cos}^2\theta^{(k)}(\boldsymbol{x})+G_{1'z}^{(k)}\mathrm{Sin}^2\theta^{(k)}(\boldsymbol{x})\end{Bmatrix} \tag{4}$$

where $G_{1'z}^{(k)}$, $G_{2z}^{(k)}$ are the transverse-shear moduli in the material coordinate system, $(1',2')$. As depicted in Fig. 1, $\theta^{(k)}(\boldsymbol{x})$ represents the fiber angle with respect to global x-axis and fibers follow a curvilinear pattern in the domain of the k-th ply, thereby resulting in zigzag functions to be defined in three-dimensional spatial coordinates, $\phi_i^{(k)}\equiv\phi_i^{(k)}(\boldsymbol{x},z)$. Herein, we have extended the original kinematic relations of RZT to account for through-the thickness stress variations of variable-stiffness composites more precisely. By preserving the original linear zigzag functions, $\phi_i^{(k)}$ used in [60], the displacement fields, $(u_i^{(k)};\ i=1,2,3)$ are expanded by incorporating quartic (fourth-order) thickness terms. They can be written by considering the thickness stretching as:

$$\begin{aligned}u_1^{(k)}(\boldsymbol{x},z)&=u_0(\boldsymbol{x})+z\theta_1(\boldsymbol{x})+z^2\kappa_1(\boldsymbol{x})+z^3\omega_1(\boldsymbol{x})+z^4L_1(\boldsymbol{x})\\&\quad+\phi_1^{(k)}(\boldsymbol{x},z)\,\psi_1(\boldsymbol{x})\end{aligned} \tag{5a}$$

$$\begin{aligned}u_2^{(k)}(\boldsymbol{x},z)&=v_0(\boldsymbol{x})-z\theta_2(\boldsymbol{x})-z^2\kappa_2(\boldsymbol{x})-z^3\omega_2(\boldsymbol{x})-z^4L_2(\boldsymbol{x})\\&\quad-\phi_2^{(k)}(\boldsymbol{x},z)\psi_2(\boldsymbol{x})\end{aligned} \tag{5b}$$

$$u_3^{(k)}(\boldsymbol{x},z)=w_0(\boldsymbol{x})+z\,w_1(\boldsymbol{x})+z^2w_2(\boldsymbol{x})+z^3w_3(\boldsymbol{x})+z^4w_4(\boldsymbol{x}) \tag{5c}$$

where the u_0 and v_0 are the uniform in-plane translations having positive directions along the x and y axes of the laminate, respectively. Moreover, the θ_1 and θ_2 are the average bending rotations around the y and x axes of the laminate and possess the positive directions shown in Fig. 1. Furthermore, the w_0 represents the average out-of-plane displacement along the positive z axis, and ψ_1, ψ_2 stand for the positive zigzag amplitudes of the RZT theory as illustrated in Fig. 1. In addition to these seven kinematic variables, which were originally used to establish the RZT, additional terms in Eqs. (5a) and (5b), χ_i $(\chi=\kappa,\omega,L;\ i=1,2)$ are defined to capture the correct in-plane displacement behavior of the curvilinear fiber laminated composite plate and this requirement will be discussed in more detail in the numerical problems section. Note that these extra terms other than the κ_1, κ_2, which physically correspond to the curvatures of the laminates, have no physical meaning. The C^3-continuity is ensured for the transverse displacement in Eq. (5c) to consider the thickness stretching. Consequently, the $w_i\,(i=1,\ldots 4)$ physically identifies the thickness stretch deformation of the laminate with varying order contributions. The linear elastic strains corresponding to the displacement fields of Eqs. (5a)–(5c) can be defined as given in the following compact form:

$$\boldsymbol{\varepsilon}^{(k)}\equiv\left\{\varepsilon_x\quad\varepsilon_y\quad\varepsilon_z\quad\gamma_{xz}\quad\gamma_{yz}\quad\gamma_{xy}\right\}^T=\boldsymbol{S}^{(k)}\,\hat{\boldsymbol{\varepsilon}} \tag{6}$$

where the terms associated with the thickness coordinate, z are collected together in a strain–displacement transformation matrix, $\boldsymbol{S}^{(k)}$, as:

$$\boldsymbol{S}^{(k)}=\begin{bmatrix}\hat{\boldsymbol{M}}_1^{(k)} & & & & & \\ & \hat{\boldsymbol{M}}_2^{(k)} & & & \mathbf{0} & \\ & & \hat{\boldsymbol{M}}_3^{(k)} & & & \\ & & & \hat{\boldsymbol{M}}_4^{(k)} & & \\ & \mathbf{0} & & & \hat{\boldsymbol{M}}_5^{(k)} & \\ & & & & & \hat{\boldsymbol{M}}_6^{(k)}\end{bmatrix} \tag{7}$$

with the transformation vectors, $\hat{\boldsymbol{M}}_i^{(k)}$ $(i=1,\ldots,6)$ which are defined explicitly as:

$$\hat{\boldsymbol{M}}_1^{(k)} = \left\{ 1 \quad z \quad z^2 \quad z^3 \quad z^4 \quad \phi_1^{(k)} \quad \phi_{1,x}^{(k)} \right\} \tag{8a}$$

$$\hat{\boldsymbol{M}}_2^{(k)} = \left\{ 1 \quad -z \quad -z^2 \quad -z^3 \quad -z^4 \quad -\phi_2^{(k)} \quad -\phi_{2,y}^{(k)} \right\} \tag{8b}$$

$$\hat{\boldsymbol{M}}_3^{(k)} = \left\{ 1 \quad 2z \quad 3z^2 \quad 4z^3 \right\} \tag{8c}$$

$$\hat{\boldsymbol{M}}_4^{(k)} = \left\{ 1 \quad 2z \quad 3z^2 \quad 4z^3 \quad \phi_{1,z}^{(k)} \quad 1 \quad z \quad z^2 \quad z^3 \quad z^4 \right\} \tag{8d}$$

$$\hat{\boldsymbol{M}}_5^{(k)} = \left\{ -1 \quad -2z \quad -3z^2 \quad -4z^3 \quad -\phi_{2,z}^{(k)} \quad 1 \quad z \quad z^2 \quad z^3 \quad z^4 \right\} \tag{8e}$$

$$\hat{\boldsymbol{M}}_6^{(k)} = \left\{ 1 \quad z \quad z^2 \quad z^3 \quad z^4 \quad \phi_1^{(k)} \quad \phi_{1,y}^{(k)} \quad 1 \quad -z \quad -z^2 \quad -z^3 \quad -z^4 \quad -\phi_2^{(k)} \quad -\phi_{2,x}^{(k)} \right\} \tag{8f}$$

where the comma notation denotes differentiation. The derivatives of the zigzag functions, $\phi_{i,x}^{(k)}$; $\phi_{i,y}^{(k)}$ $(i = 1, 2)$ in Eqs. (8a), (8b) and (8f) become a varying function of in-plane coordinates among all terms. Although this terms naturally vanish when modelling laminates with straight fibers, the contribution of these terms while calculating the in-plane strains of curvilinear fiber laminates may not be disregarded. In Eq. (6), the $\hat{\boldsymbol{\varepsilon}}$ vector is a generalized strain vector, $\hat{\boldsymbol{\varepsilon}} = \{ \hat{\varepsilon}_1 \quad \hat{\varepsilon}_2 \quad \hat{\varepsilon}_3 \quad \hat{\varepsilon}_4 \quad \hat{\varepsilon}_5 \quad \hat{\varepsilon}_6 \}^T$ and contains the following strain measures:

$$\hat{\boldsymbol{\varepsilon}}_1 = \{ u_{0,x} \quad \theta_{1,x} \quad \kappa_{1,x} \quad \omega_{1,x} \quad L_{1,x} \quad \psi_{1,x} \quad \psi_1 \}^T \tag{9a}$$

$$\hat{\boldsymbol{\varepsilon}}_2 = \{ v_{0,y} \quad \theta_{2,y} \quad \kappa_{2,y} \quad \omega_{2,y} \quad L_{2,y} \quad \psi_{2,y} \quad \psi_2 \}^T \tag{9b}$$

$$\hat{\boldsymbol{\varepsilon}}_3 = \{ w_1 \quad w_2 \quad w_3 \quad w_4 \}^T \tag{9c}$$

$$\hat{\boldsymbol{\varepsilon}}_4 = \{ \theta_1 \quad \kappa_1 \quad w_1 \quad L_1 \quad \psi_1 \quad w_{0,x} \quad w_{1,x} \quad w_{2,x} \quad w_{3,x} \quad w_{4,x} \}^T \tag{9d}$$

$$\hat{\boldsymbol{\varepsilon}}_5 = \{ \theta_2 \quad \kappa_2 \quad w_2 \quad L_2 \quad \psi_2 \quad w_{0,y} \quad w_{1,y} \quad w_{2,y} \quad w_{3,y} \quad w_{4,y} \}^T \tag{9e}$$

$$\hat{\boldsymbol{\varepsilon}}_6 = \{ u_{0,y} \quad \theta_{1,y} \quad \kappa_{1,y} \quad w_{1,y} \quad L_{1,y} \quad \psi_{1,y} \quad \psi_1 \quad v_{0,x} \quad \theta_{2,x} \kappa_{2,x} \quad w_{2,x} \quad L_{2,x} \quad \psi_{2,x} \quad \psi_2 \}^T \tag{9f}$$

Note that the kinematic variables in Eqs. (9a)–(9f) are only the functions of the in-plane coordinates, which make the generalized strain vector, $\hat{\boldsymbol{\varepsilon}}$ be independent from the thickness coordinate, z for the following calculations. Introducing Eq. (6) into the standard Hooke stress–strain relationship for the k-th orthotropic layer yields:

$$\boldsymbol{\sigma}^{(k)} = \boldsymbol{D}^{(k)} \, \boldsymbol{\varepsilon}^{(k)} \equiv \boldsymbol{D}^{(k)} \, \boldsymbol{S}^{(k)} \, \hat{\boldsymbol{\varepsilon}} \tag{10}$$

where $\boldsymbol{D}^{(k)}$ is the standard k-th layer constitutive matrix relating stress and strains. The $\boldsymbol{D}^{(k)}$, whose elements are given explicitly in Appendix A, is not a fixed matrix as is usual in straight fibers. It is a function of the fiber angle, $\theta^{(k)}$ and the angle varies according to x and y, so it differs for each element in the x-y domain. By taking the variation of the internal strain energy, δU_i and substituting Eq. (6) and Eq. (10) for the strain and stresses, respectively gives

$$\delta U_i = \iiint \left(\delta \boldsymbol{\varepsilon}^{(k)} \right)^T \boldsymbol{\sigma}^{(k)} dx \, dy \, dz = \iint \left(\delta \hat{\boldsymbol{\varepsilon}} \right)^T \hat{\boldsymbol{D}} \, \hat{\boldsymbol{\varepsilon}} \, dx \, dy \tag{11}$$

where the generalized constitutive matrix, $\hat{\boldsymbol{D}}$ is defined as

$$\hat{\boldsymbol{D}} = \int \left(\boldsymbol{S}^{(k)} \right)^T \boldsymbol{D}^{(k)} \, \boldsymbol{S}^{(k)} dz = \sum_{k=1}^{N_L} \int_{z_k}^{z_{k+1}} \left(\boldsymbol{S}^{(k)} \right)^T \boldsymbol{D}^{(k)} \, \boldsymbol{S}^{(k)} dz \tag{12}$$

3. Non-Uniform Rational B-Splines (NURBS)

Complex geometries can be represented exactly in today's computer aided design (CAD) technology which is based on NURBS basis functions. By using bivariate NURBS basis functions, $R_{ij}^{pq}(\xi, \eta)$ and associated control points coordinate matrix, $\boldsymbol{B}_{ij}$, a NURBS surface, illustrated in Fig. 2, can be constructed as:

$$\boldsymbol{S}(\xi, \eta) = \sum_{i=1}^{n} \sum_{j=1}^{m} R_{ij}^{pq}(\xi, \eta) \boldsymbol{B}_{ij} = \sum_{i=1}^{n} \sum_{j=1}^{m} \frac{N_i^p(\xi) N_j^q(\eta) w_{ij}}{\sum_{k=1}^{n} \sum_{l=1}^{m} N_k^p(\xi) N_l^q(\eta) w_{kl}} \boldsymbol{B}_{ij} \tag{13}$$

where $N_i^p(\xi)$, $N_j^q(\eta)$ are the univariate B-spline basis functions of degree p and q defined in the ξ and η directions of the parametric space, respectively. Additionally, w_{ij} stand for the associated control point weight, and it provides opportunity to the points over the surface, $\boldsymbol{S}(\xi, \eta)$ to move closer to (farther from) $\boldsymbol{B}_{ij}$ with the increase (decrease) of the weight.

Fig. 2 shows a biquadratic ($p = q = 2$) NURBS surface and its control mesh with the knot vectors $\boldsymbol{U}(\xi) = \boldsymbol{V}(\eta) = \{0.\ 0.\ 0.\ 0.333\ 0.666\ 1.\ 1.\ 1.\}$. As depicted in Fig. 2, there are two types of meshes in NURBS terminology which are the physical and the control mesh. The first one is a similar mesh of standard finite element analysis (FEA) where the physical domain is divided into elements, i.e., 3 × 3 mesh. The latter one is like a scaffold where the control points (blue rectangles) lie on and controls the shape of the geometry. The distinction between the control points and the nodes of standard FEA is that only the first and last control points of a NURBS surface coincide with the physical domain whereas all nodes lie on the geometry in the FEA. The B-spline functions, $N_i^p(\xi)$; $N_j^q(\eta)$ encountered in Eq. (13) can be defined by the following Cox-de Boor recursion formulas [48] as:

$$N_i^0(\xi) = \begin{cases} 1 & \text{if } \xi_i \leqslant \xi \leqslant \xi_{i+1} \\ 0 & \text{otherwise} \end{cases} \tag{14a}$$

and

$$N_i^p(\xi) = \frac{\xi - \xi_i}{\xi_{i+p} - \xi_i} N_i^{p-1}(\xi) + \frac{\xi_{i+p+1} - \xi}{\xi_{i+p+1} - \xi_{i+1}} N_{i+1}^{p-1}(\xi) \tag{14b}$$

where the values of ξ_i and η_j are elements of the knot vectors, $\boldsymbol{U}$, $\boldsymbol{V}$ which have non-decreasing set of coordinates in the parameter spaces and can be written as

$$\boldsymbol{U} = \{ \xi_1, \ \xi_2, \ \cdots, \ \xi_i, \cdots, \xi_{n+p+1} \} \tag{15a}$$

$$\boldsymbol{V} = \{ \eta_1, \ \eta_2, \ \cdots, \ \eta_j, \cdots, \eta_{m+q+1} \} \tag{15b}$$

where n and m denote the number of control points and B-spline basis functions in ξ, η directions, respectively. The non-zero knot intervals, $[\xi_i, \xi_{i+1}) \otimes [\eta_j, \eta_{j+1})$ in the above knot vectors are called as knot spans which define the element domains. A special feature of B-splines is that $(p + 1)$ of $N_i^p(\xi)$ and $(q + 1)$ of $N_j^q(\eta)$ are nonzero functions, $(N_{i-p}^p, \ldots, N_i^p) \otimes (N_{j-q}^q, \ldots, N_j^q)$ in any given knot span, $[\xi_i, \xi_{i+1}) \otimes [\eta_j, \eta_{j+1})$.Therefore, the total number of control points and

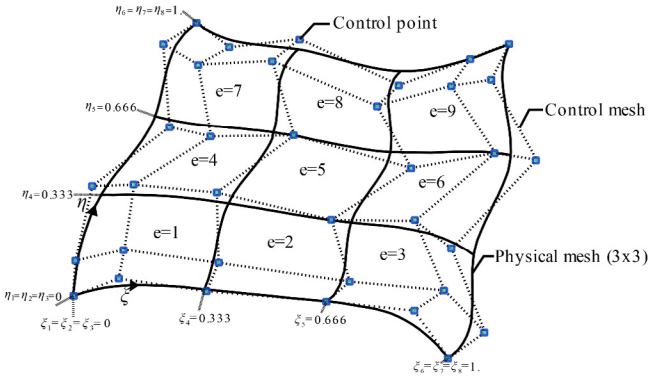

Fig. 2. Biquadratic ($p = q = 2$) NURBS surface with the control mesh.

B-spline basis functions per element is $n \times m = (p+1) \times (q+1)$ for 2D analysis.

4. Isogeometric Refined zigzag formulation (IG-RZT)

Hughes et al. [49] have recently introduced the isogeometric analysis (IGA) to integrate the FEA with CAD systems which use NURBS functions to represent the exact geometry. Instead of using conventional Lagrangian or Hermitian type polynomial functions of FEA, IGA uses NURBS functions in both discretization of the displacement fields and geometry. In this context, by defining a global index as $I = n(j-1)+i$ and rewriting Eq. (13) in a more compact form, the geometry of the IG-RZT element can be discretized as:

$$\boldsymbol{S}^{(e)} = \left\{ x^{(e)}(\xi,\eta) \quad y^{(e)}(\xi,\eta) \right\}^T = \sum_{I=1}^{n\times m} R_I(\xi,\eta) \left\{ x_I^{(e)} \quad y_I^{(e)} \right\}^T \tag{16}$$

where $x_I^{(e)}; y_I^{(e)}$ represent the physical coordinates of the I-th control point in the e-th element. In a similar fashion, the unknown kinematic variables in the eth element can be discretized as:

$$\begin{aligned} \boldsymbol{u}^{(\mathbf{e})} &= \{ u_0 \;\; \theta_1 \;\; \kappa_1 \;\; \omega_1 \;\; L_1 \;\; \psi_1 \;\; v_0 \;\; \theta_2 \;\; \kappa_2 \;\; \omega_2 \;\; L_2 \;\; \psi_2 \;\; w_0 \;\; w_1 \;\; w_2 \;\; w_3 \;\; w_4 \}^T \\ &= \sum_{I=1}^{nxm} R_I(\xi,\eta)\, \boldsymbol{a}_I^{(e)} \end{aligned} \tag{17}$$

with $\boldsymbol{a}_I^{(e)}$ representing the local displacement vector of the I-th control point that is defined as:

$$\boldsymbol{a}_I^{(e)} = \{ u_0^I \;\; \theta_1^I \;\; \kappa_1^I \;\; \omega_1^I \;\; L_1^I \;\; \psi_1^I \;\; v_0^I \;\; \theta_2^I \;\; \kappa_2^I \;\; \omega_2^I \;\; L_2^I \;\; \psi_2^I \;\; w_0^I \;\; w_1^I \;\; w_2^I \;\; w_3^I \;\; w_4^I \}^T \tag{18}$$

Then, the generalized strain vector, $\hat{\boldsymbol{\varepsilon}}^{(e)}$ in Eqs. (9a)–(9f) can be expressed as:

$$\begin{aligned} \hat{\boldsymbol{\varepsilon}}^{(e)} &= [\boldsymbol{B}_1 \;\; \ldots \;\; \boldsymbol{B}_I \;\; \ldots \;\; \boldsymbol{B}_{n\times m}] \{ \boldsymbol{a}_1 \;\; \ldots \;\; \boldsymbol{a}_I \;\; \ldots \;\; \boldsymbol{a}_{n\times m} \}^T \\ &\equiv \boldsymbol{B}\, \boldsymbol{a}^{(e)} \end{aligned} \tag{19a}$$

with

$$\boldsymbol{B}_I = \left[\boldsymbol{B}_I^1 \;\; \boldsymbol{B}_I^2 \;\; \boldsymbol{B}_I^3 \;\; \boldsymbol{B}_I^4 \;\; \boldsymbol{B}_I^5 \;\; \boldsymbol{B}_I^6 \right]^T \tag{19b}$$

where the matrices $\boldsymbol{B}_I^{\alpha}$ $(\alpha = 1, 2, \ldots, 6)$ contain the derivatives of the NURBS shape functions and the explicit form of these matrices are provided in Appendix B. Substituting Eq. (19a) into Eq. (11), the variational form of internal strain energy yields:

$$\delta U_i = \iint \left(\delta \hat{\boldsymbol{\varepsilon}}^{(e)} \right)^T \hat{\boldsymbol{D}}\, \hat{\boldsymbol{\varepsilon}}^{(e)} dx\, dy \equiv \left(\delta \boldsymbol{a}^{(e)} \right)^T \boldsymbol{K}^{(e)}\, \boldsymbol{a}^{(e)} \tag{20}$$

where the element stiffness matrix, $\boldsymbol{K}^{(e)}$ is defined as

$$\boldsymbol{K}^{(e)} = \int \int \boldsymbol{B}^T \hat{\boldsymbol{D}}\, \boldsymbol{B}\; dx\, dy \tag{21}$$

The integration domain of Eq. (21), $dxdy$ needs to be mapped onto the parametric domain, $d\xi d\eta$ since the integrand is defined in the parametric space. Transformation from parametric space to physical one can be carried out by defining the Jacobian, $\mathbf{J}$ using Eq. (16) as:

$$\boldsymbol{J} = \begin{bmatrix} \frac{\partial x}{\partial \xi} & \frac{\partial y}{\partial \xi} \\ \frac{\partial x}{\partial \eta} & \frac{\partial y}{\partial \eta} \end{bmatrix} \tag{22}$$

By using the determinant of the $\mathbf{J}$ matrix, Eq. (21) can be rewritten as:

$$\boldsymbol{K}^{(e)} = \int \int \boldsymbol{B}^T \hat{\boldsymbol{D}}\, \boldsymbol{B}\, \det \boldsymbol{J}\, d\xi\, d\eta \tag{23}$$

To be able to numerically calculate Eq. (23), one can use Gauss Quadrature method. Consequently, the parametric domain should be transformed with relevant Jacobian mapping to parent element domain, $\left(\tilde{\xi}, \tilde{\eta}\right) = [-1,1] \otimes [-1,1]$. Such transformation can be readily performed using the preliminaries of IGA [50]. In addition, the variational form of the strain energy caused by the externally applied transverse pressure, $q_z(x,y)$, can be defined for IG-RZT element as:

$$\delta U_e = \iint q_z(x,y)\, \delta u_3^{(k)}(x,y,z=h)\, dx\, dy \tag{24a}$$

or

$$\delta U_e = \iint q_z(x,y) \left(\delta w_0 + h\delta w_1 + h^2 \delta w_2 + h^3 \delta w_3 + h^4 \delta w_4 \right) dx\, dy = \left(\delta \boldsymbol{a}^{(e)} \right)^T \boldsymbol{f}^{(e)} \tag{24b}$$

where $\boldsymbol{f}^{(e)}$ is the force vector of all control points belonging to IG-RZT element which can be written as:

$$\boldsymbol{f}^{(e)} = \left\{ \mathbf{0} \;\; f_1^{(e)} \;\; \ldots \;\; \mathbf{0} \;\; f_I^{(e)} \;\; \ldots \;\; \mathbf{0} \;\; f_{n\times m}^{(e)} \right\}; I = 1, \ldots, n \times m \tag{25}$$

with the nonzero load (transverse pressure) vector for the I-th control point:

$$\begin{aligned} \boldsymbol{f}_I^{(e)} &= \left\{ f_{w_0}^I \;\; f_{w_1}^I \;\; f_{w_2}^I \;\; f_{w_3}^I \;\; f_{w_4}^I \right\}^T \\ &= \iint q_z(\xi,\eta)\, R_I(\xi,\eta) \left\{ 1 \;\; h \;\; h^2 \;\; h^3 \;\; h^4 \right\}^T \det \boldsymbol{J}\, d\xi\, d\eta \end{aligned} \tag{26}$$

Equating the internal and external strain energies, the principal of virtual work can be defined as:

$$\delta U_i = \delta U_e \rightarrow \left(\delta \boldsymbol{a}^{(e)} \right)^T \left(\boldsymbol{K}^{(e)} \boldsymbol{a}^{(e)} - \boldsymbol{f}^{(e)} \right) = 0 \tag{27}$$

which results in the final set of static equilibrium equations for an IG-RZT element:

$$\boldsymbol{K}^{(e)} \boldsymbol{a}^{(e)} = \boldsymbol{f}^{(e)} \tag{28}$$

Here, it is important to note that the Eq. (28) can be defined for all the isogeometric elements properly and these equations can be assembled utilizing the connectivity of the elements in a global system of equations. Finally, applying the problem specific boundary conditions into the global set of equations, the unknown displacement DOF can be evaluated and subsequently utilized for predicting the three-dimensional deformations and stresses in the physical geometry. However, RZT predicts the transverse shear stresses accurately in a piecewise constant manner throughout the thickness direction of a laminate and the lack of obtaining a continuous, through the thickness transverse shear stress distribution with RZT can be overcome by using Cauchy's equilibrium equations and high order NURBS functions. The integration of Cauchy's equilibrium equations yields the transverse shear stress distributions to be obtained as:

$$\tau_{xz}^{(k)}(x,y,z) = -\int_{-h}^{z} \frac{\partial \sigma_x^{(k)}}{\partial x} dz - \int_{-h}^{z} \frac{\partial \tau_{xy}^{(k)}}{\partial y} dz + f_0^{(k)}(x,y) \tag{29a}$$

$$\tau_{yz}^{(k)}(x,y,z) = -\int_{-h}^{z} \frac{\partial \sigma_y^{(k)}}{\partial y} dz - \int_{-h}^{z} \frac{\partial \tau_{xy}^{(k)}}{\partial x} dz + f_1^{(k)}(x,y) \tag{29b}$$

The integration constants of the first and last layers, $f_0^{(k=1,N_L)}$, $f_1^{(k=1,N_L)}$ in Eqs. (29a) and (29b) can be obtained by imposing the zero transverse shear stresses at the outer edges of the plate which can be stated mathematically as:

$$\tau_{xz}^{(k=1)}(x,y,z=-h) = \tau_{xz}^{(k=N_L)}(x,y,z=h) = 0 \tag{30a}$$

$$\tau_{yz}^{(k=1)}(x,y,z=-h) = \tau_{yz}^{(k=N_L)}(x,y,z=h) = 0 \tag{30b}$$

which results in

$$f_0^{(k)} = \left(\int_{-h}^{z} \frac{\partial \sigma_x^{(k)}}{\partial x} dz \right)\Big|_{z=\alpha} + \left(\int_{-h}^{z} \frac{\partial \tau_{xy}^{(k)}}{\partial y} dz \right)\Big|_{z=\alpha} \tag{31a}$$

$$\begin{aligned} f_1^{(k)} &= \left(\int_{-h}^{z} \frac{\partial \sigma_y^{(k)}}{\partial y} dz \right)\Big|_{z=\alpha} + \left(\int_{-h}^{z} \frac{\partial \tau_{xy}^{(k)}}{\partial x} dz \right)\Big|_{z=\alpha} \\ &(k = 1, N_L;\; \alpha = -h, \; +h) \end{aligned} \tag{31b}$$

Additionally, the interlaminar transverse shear stress continuity can be written as

$$\tau_{xz}^{(k)}(z=z_{k+1}) = \tau_{xz}^{(k+1)}(z=z_{k+1}) \tag{32a}$$

$$\tau_{yz}^{(k)}(z=z_{k+1}) = \tau_{yz}^{(k+1)}(z=z_{k+1}) \quad (k=1,\ \ldots\ ,N_L-1) \tag{32b}$$

and can be used for the other integration constants of the interior layers which yields

$$f_0^{(k)} = f_0^{(k-1)} - \left(\int_{-h}^{z}\sigma_{x,x}^{(k-1)}dz\right)\Big|_{z=z_k} - \left(\int_{-h}^{z}\tau_{xy,y}^{(k-1)}dz\right)\Big|_{z=z_k} + \left(\int_{-h}^{z}\sigma_{x,x}^{(k)}dz\right)\Big|_{z=z_k} + \left(\int_{-h}^{z}\tau_{xy,y}^{(k)}dz\right)\Big|_{z=z_k} \tag{33a}$$

$$f_1^{(k)} = f_1^{(k-1)} - \left(\int_{-h}^{z}\sigma_{y,y}^{(k-1)}dz\right)\Big|_{z=z_k} - \left(\int_{-h}^{z}\tau_{xy,x}^{(k-1)}dz\right)\Big|_{z=z_k} + \left(\int_{-h}^{z}\sigma_{y,y}^{(k)}dz\right)\Big|_{z=z_k} + \left(\int_{-h}^{z}\tau_{xy,x}^{(k)}dz\right)\Big|_{z=z_k} \tag{33b}$$

with $k=2,\ \ldots\ ,N_L$.

5. Numerical results

In this section, numerical analysis of multi-layered composites and sandwich plates with curvilinear fibers are performed using NURBS based isogeometric approach in conjunction with RZT. Then, the displacement and stress results predicted by using IG-RZT are compared and validated with respect to the reference solutions that are either generated using ANSYS or available in literature. Here, a total of three cases have been examined, and the first two of them are selected from literature in order to compare the present IG-RZT element with existing problems. Therefore, the assumptions made in the references of the first two cases are still valid here, and the excessive spacing between fibers or overlapping due to the given fiber orientation has been neglected in the analyzes. The third case is a new example added to the literature to emphasize the importance of isogeometric analysis and to make the defined fiber orientation actually applicable.

5.1. A square curvilinear fiber laminate subjected to uniform pressure

In this first validation case (Case a), a tow-steered, laminated square plate ($a=b=1\,\mathrm{m}$) from Tornabene et al. [47] has been analyzed using the proposed isogeometric formulation. Tornabene et al. [47] have examined this problem under static load according to the Carrera's Unified Formulation (CUF). By imposing CUF in [47], they have the ability to employ different thickness functions, as well as the zigzag effect based on either ESL or layerwise approach. Instead of using finite elements, the governing equation system in [47], has been solved numerically through the Generalized Differential Quadrature (GDQ) method. Since the ESL approach has been used in the present IG-RZT study, the results obtained have been compared with ED3 of [47] which stands for (E)SL-(D)isplacement based theory with the third order thickness functions in the displacement field. The plate is subjected to a uniform pressure, $q_z(z=h) = -10\,[kPa]$ with clamped boundary conditions on its all edges The laminate, made of two layers of equal thickness and has span to thickness ratio which covers a range of 10, 25 and 40. The material is carbon/epoxy with the following elastic properties:

$$(E_{1'1'},\ E_{2'2'},\ E_{3'3'},\ G_{1'2'},\ G_{1'3'},\ G_{2'3'}) = (137.9,\ 8.96,\ 8.96,\ 7.1,\ 7.1,\ 6.21)\ GPa \tag{34a}$$

$$(\nu_{1'2'},\ \nu_{1'3'},\ \nu_{2'3'}) = (0.3,\ 0.3,\ 0.49) \tag{34b}$$

This two-layered tow steered plate has also been studied by Demasi et al. [44] using Murakami's zigzag functions [11] with the standard triangular plate finite elements. Despite the fact that Demasi et al. [44] have used the theory-invariant Generalized Unified Formulation (GUF), which enables to define different theories for all the three displacement fields, the present IG-RZT approach has been compared with ${}_{ZZZ}PVD_{444}$ in [44]. The left subscript letters ZZZ in this notation mean Murakami's zigzag theory is adopted for all x, y, z displacement fields and the right subscript 444 indicates the order of expansions, respectively. The notation used in [44] to describe the fiber angle with respect to x axis, $\theta^{(k)}$ is given as:

$$\theta^{(k)} = \frac{2\left(T_1^k - T_0^k\right)}{a}|x| + T_0^k \tag{35}$$

where T_0^k and T_1^k stand for the angles of the kth layer fibers with respect to x axis at $x=0$ (center) and $x=\pm a/2$(edge), respectively. Since the span to thickness ratio of the plates studied in references [44,47] was limited to 10, the 3-D solution of ANSYS with Solid 185 brick elements has been used to confirm the analyses for the other span to thickness ratios. A solid mesh of 80x80x40 is generated in ANSYS, where 80 and 40 elements uniformly subdivide the plate edges (a, and b) and thickness edge, in the given order. The displacement and stress results of the analyses are expressed in $[m]$, $[Pa]$, respectively and obtained at the point $P(x=0.25a, y=0.25b, z)$ for the following four cases where the fiber orientation details and the patterns of those are listed in Table 1 and depicted in Fig. 3, respectively.

The importance of the selected degree for the thickness function, z and its effect on the in-plane stresses is shown in Fig. 4. Additionally, the legend terms "ez" in Figs. 4–7 and "ez0" in Fig. 7, denote that the transverse normal strain is considered or not in the analyses, respectively. As shown in Fig. 4, the correct distribution of the in-plane stresses cannot be captured by using linear ($z1$) or quadratic ($z2$) expansion of NURBS thickness functions. It is evident from Fig. 4 that at least a cubic ($z3$) thickness function needs to be considered in the displacement approximation to model fairly correct trend of in-plane stresses through the thickness. As depicted in Fig. 4; the in-plane stress results, obtained from the fourth order thickness function ($z4$), are in excellent agreement with the reference solution Demasi et al. [44] and slightly differs from Tornabene et al. [47]. It is also inferred from Fig. 5 that the in-plane and transverse displacement results predicted by the present approach are in well agreement with those obtained in [44]. Fig. 5c also explains the reason of slight stress discrepancies between IG-RZT and [47] as such the transverse displacement is underestimated using the approach of [47].

The convergence analysis of σ_{xx} shown in Fig. 6 indicates that a third order ($p=3$) NURBS interpolation for in-plane displacements requires less total degrees of freedom (DOF) than those of the second order ($p=2$) NURBS functions. As for convergence rate of axial stress in Fig. 6, the convergence capability of present IGRZT-z4ez element with p degree, 3 is higher than other solutions such that the IG-RZT approach requires approximately 38% less DOF than that of [44] for convergent axial stress.

Fig. 7 shows the effect of thickness stretching on the through the thickness normal stress distributions where the transverse normal strains are retained (ez) or removed (ez0) from the kinematic assumptions. It is clear from Fig. 7 that discarding ε_{zz} in the calculations result

Table 1
Definitions of the curvilinear fiber paths for different analysis cases a.

Case	$\left\langle T_1^{(1)}\middle\vert T_0^{(1)}\right\rangle$ $\left\langle T_1^{(2)}\middle\vert T_0^{(2)}\right\rangle$*
a1	⟨90|90⟩ ⟨0|0⟩
a2	⟨90|75⟩ ⟨0|15⟩
a3	⟨90|60⟩ ⟨0|30⟩
a4	⟨90|45⟩ ⟨0|45⟩

* Notation is deduced from Ref. [44] and the superscripts of the fiber angles represent for which layer they belong to.

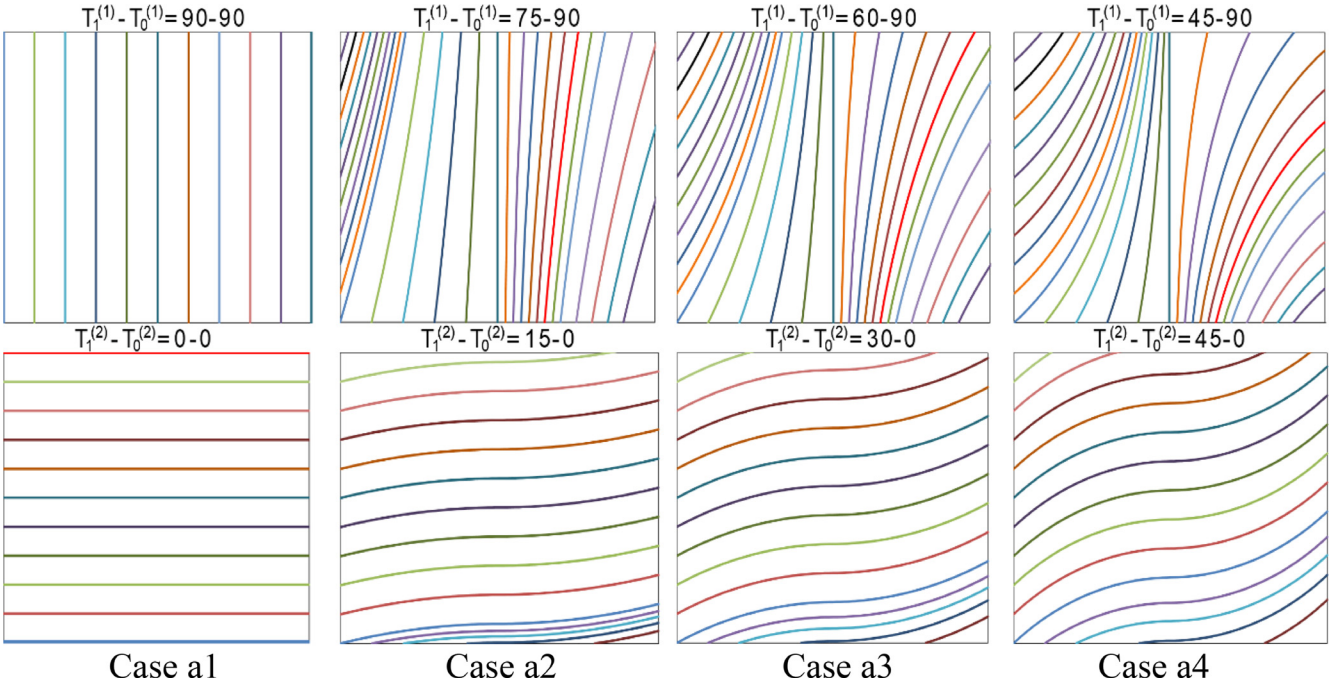

Fig. 3. Curvilinear fiber patterns of the two-layer laminated square plate (Case a).

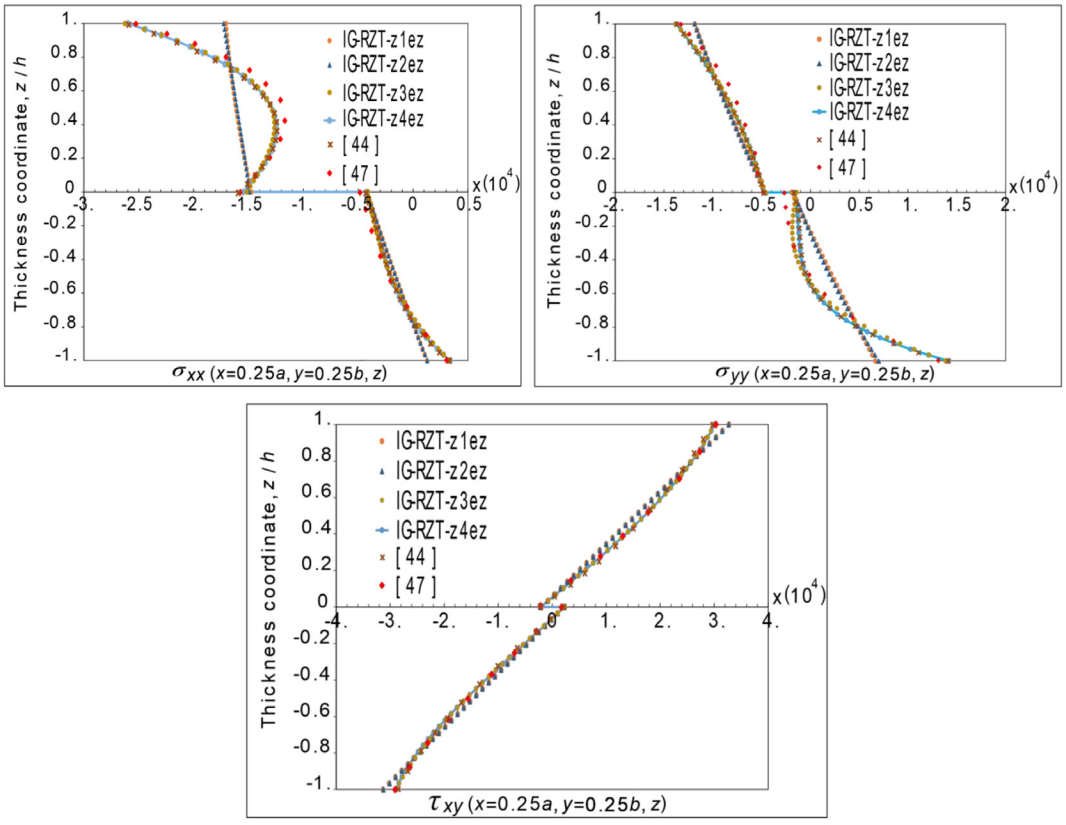

Fig. 4. Comparison between through the thickness polynomial expansions of IG-RZT (Case a4-$a/2h = 10$).

in a larger error when compared with the reference Demasi et al. [44] solution and it supports the statements of Koiter [61] and Carrera et al. [62] which are about the meaningless of including additional in-plane variables if the thickness stretching is not considered. Hence, in the remaining analyses, unless otherwise stated, the transverse normal strain is taken into account and through the thickness polynomial expansion, in-plane NURBS degree and the total DOF is selected as $z4$, $p = 3$ and 20825, respectively.

The distributions of normal and transverse shear stress components through the thickness direction, z are illustrated in Fig. 8 for the four

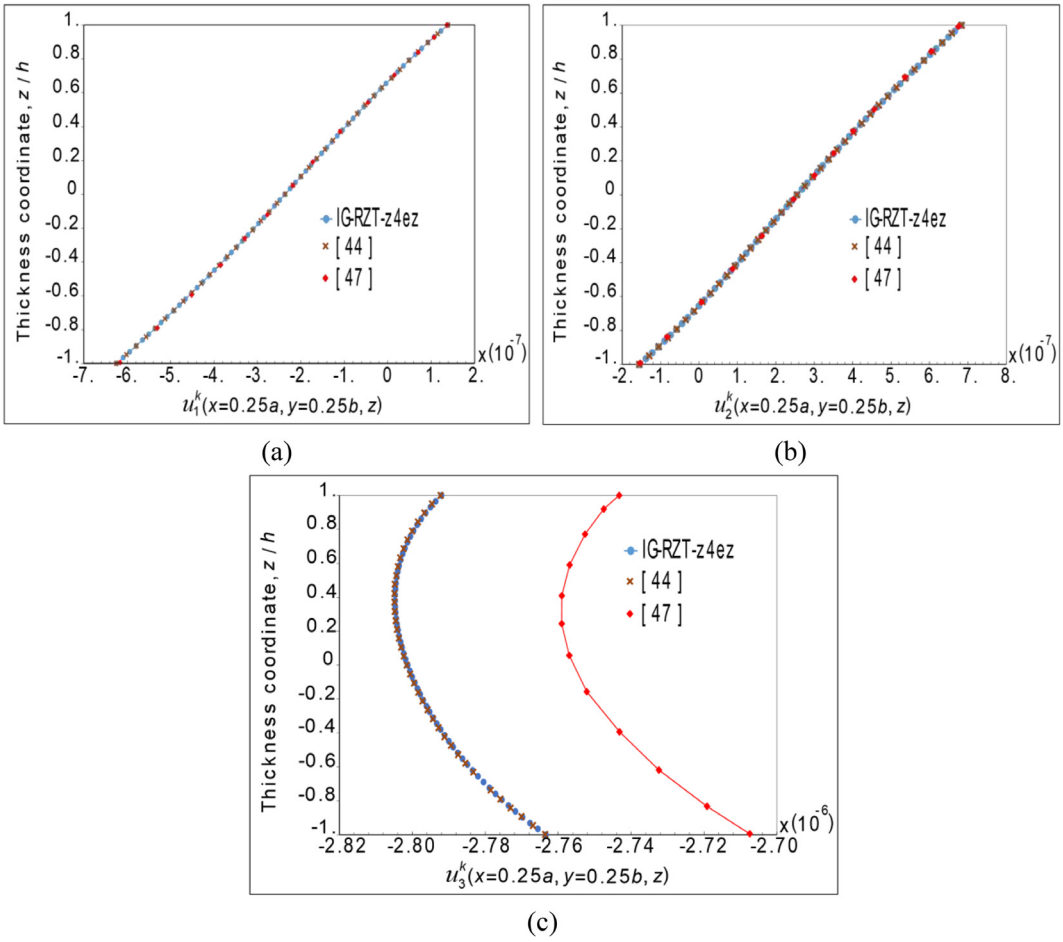

Fig. 5. Comparison of in-plane a) $u_1^{(k)}$, b) $u_2^{(k)}$ and transverse displacements c) $u_3^{(k)}$ through the thickness direction (Case a4 – $a/2h = 10$).

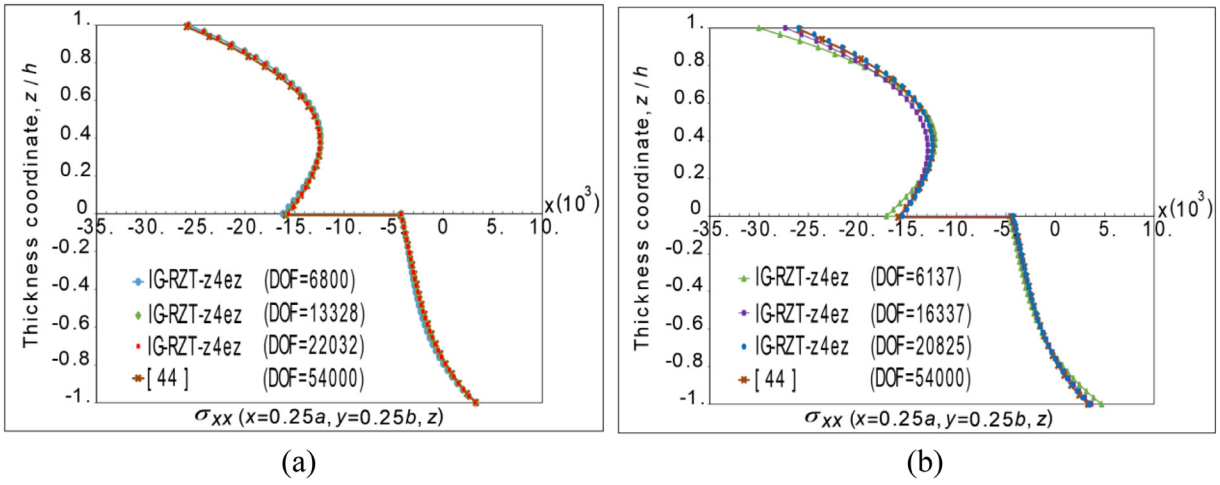

Fig. 6. Convergence analysis of normal stress, σ_{xx} for Case a4 ($a/2h = 10$) with different in-plane NURBS degrees, a) $p = 2$ and b) $p = 3$.

different fiber orientation cases (Case a1-a4). These results demonstrate that the stresses predicted by IG-RZT are almost indistinguishable from those of reference solutions generated using ANSYS, thereby confirming superior accuracy of IG-RZT formulation for VAT composite structures. Note that the transverse shear stress distributions presented in these figures are obtained from Cauchy's equilibrium equations. Hence, utilization of third order NURBS basis functions within IG-RZT methodology can allow one to accurately estimate through-the-thickness distribution of transverse shear stresses, even in the case of modelling variable angle tow composites. Additionally, in Fig. 9, we present the in-plane normal and transverse shear stresses for various values of span to thickness ratios. Remarkably, these results indicate that the IG-RZT stress predictions overlap with those of ANSYS continuum model even for very thin/thick VAT composites. Besides, Fig. 10 reveals the complexity of in-plane normal and shear stress contours for Case a4, which is well predicted by IG-

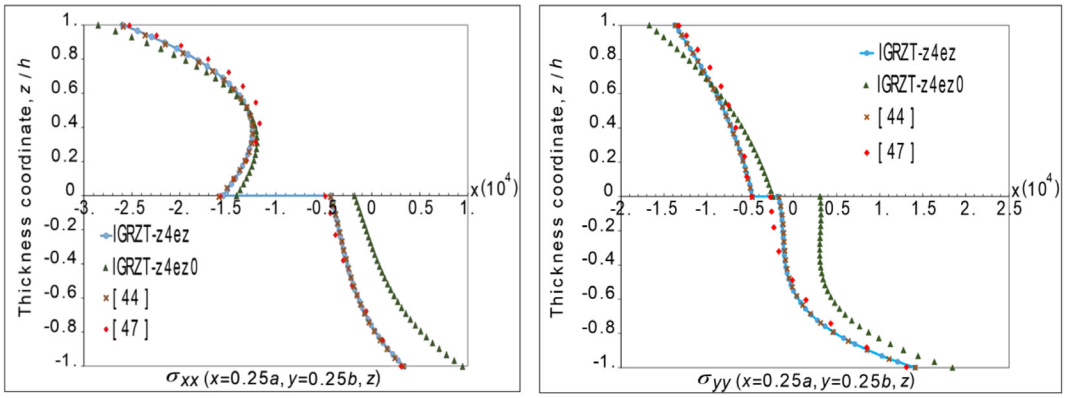

Fig. 7. Effect of transverse normal strain, ε_{zz} on the in-plane normal stresses, a) σ_{xx} and b) σ_{yy}

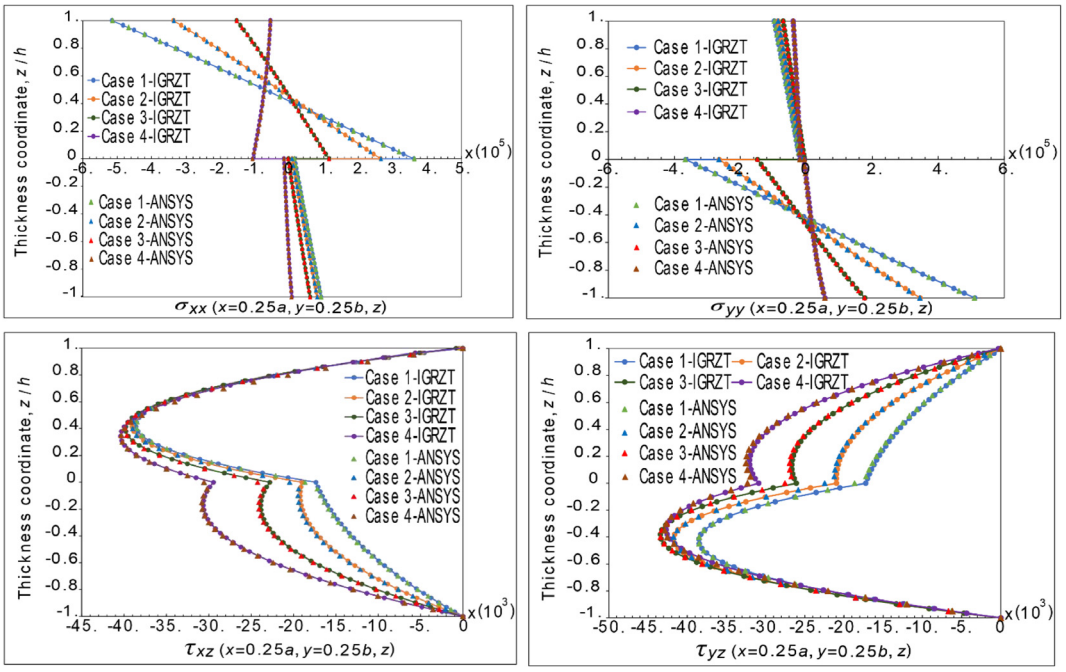

Fig. 8. Through the thickness normal (top) and transverse shear stress (bottom) distributions for various cases (a/2h = 25).

RZT methodology. Overall, the displacement and stress results discussed herein validate and prove that the IG-RZT framework can be an attractive numerical-analysis platform for modelling complex mechanics of VAT composite structures.

5.2. A three-layer sandwich plate with curvilinear fibers

To further assess the accuracy of the present IG-RZT formulation, the bending analysis of a three-layer sandwich plate problem (Case b) from Tornabene and Bacciocchi [45] has been revisited. This sandwich structure is a square plate ($a = b = 1.5\,\mathrm{m}$) subjected to a uniform pressure, $q_z(z = h) = -10\,[kPa]$ with clamped boundary conditions on its all edges. The face sheets of sandwich plate are made of curvilinear glass–epoxy fibers and the core of sandwich laminate is considered as an isotropic material. The mechanical properties of these materials are listed in Table 2. The thickness of the laminae for the sandwich structure are 0.02/0.06/0.02 $[m]$ and the laminate has span to thickness ratio of 15. The curvilinear fiber orientations of the sandwich outer skins are defined as:

$$\theta^{(k=1)} = \phi^{(k=1)}\Omega^{(k=1)} \tag{36a}$$

$$\theta^{(k=3)} = 90 + \phi^{(k=3)}\Omega^{(k=3)} \tag{36b}$$

where

$$\Omega^{(k=1)} = \Omega^{(k=3)} = \mathrm{Sin}\left(\pi\left(\frac{x}{a} + 0.5\right)\right) \tag{37}$$

Four different case studies are established by changing values of the $\phi^{(k)}$ constant as listed in Table 3. For clarity, the curvilinear path planning of all cases are depicted in Fig. 11.

Fig. 12 displays through-the-thickness zigzag variations of in-plane displacements obtained by IG-RZT for each four cases. As is clear from Fig. 12 that in-plane displacements vary according to the braiding density over the center of the laminate as illustrated in Fig. 11. This expected behavior can be elaborated as follows. The fiber alignments of Case b4 results in a dramatic decrease of the first- and third-layers stiffness through the x and y directions, as compared to the ones of other cases. This curvilinear fiber distribution elucidates the reason why Case b4 (blue circle in Fig. 12a) experiences maximum and min-

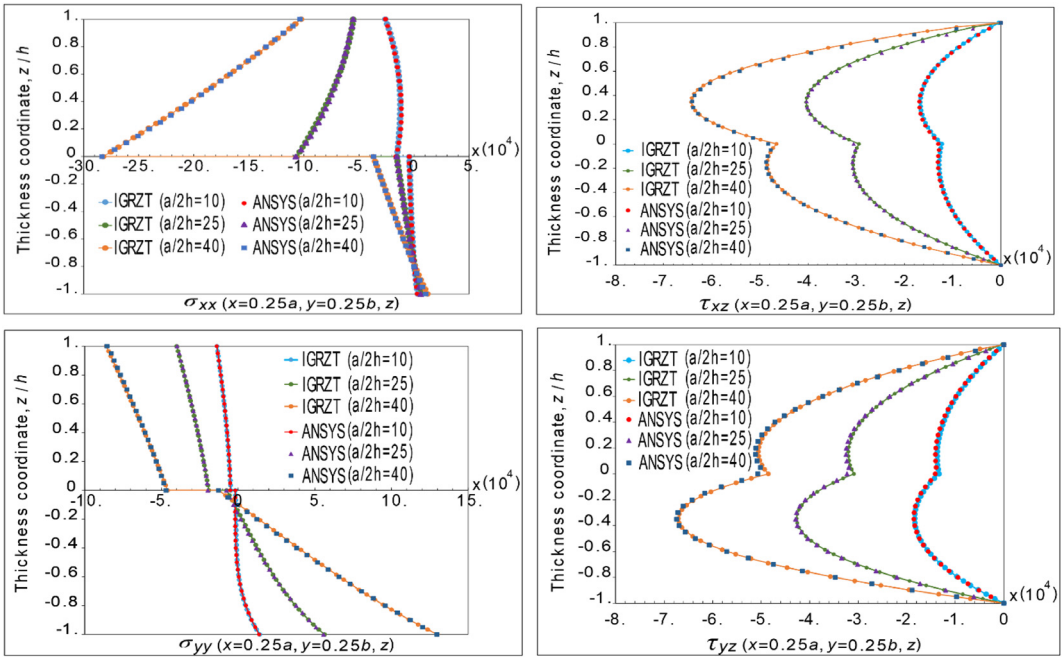

Fig. 9. Variation of normal (left) and transverse shear stress (right) distributions for $a/2h = 10$, 25 and 40 (Case a4).

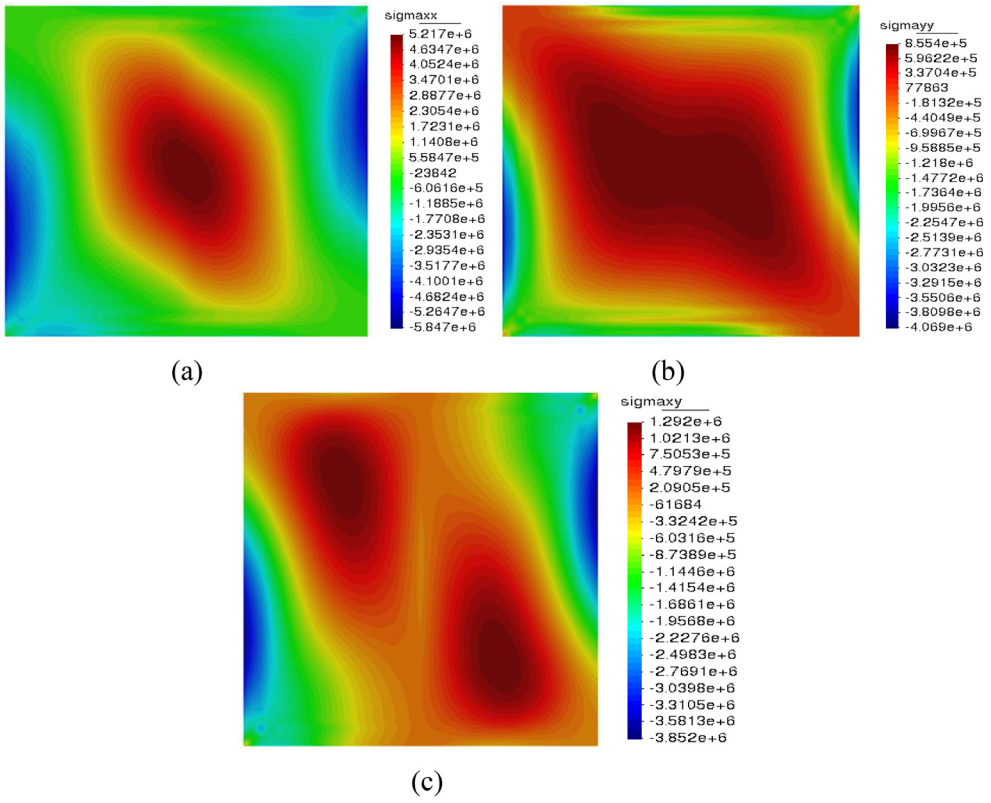

Fig. 10. In-plane $(x, y, z = h)$ stress a) σ_{xx}, b) σ_{yy} and c) τ_{xy} contour plots (Case a4-$a/2h = 40$).

Table 2
Mechanical properties of the materials used in Case b.

Material	Young's Moduli [GPa]	Poisson's Ratios	Shear Moduli
Glass-epoxy	$E_{1'} = 53.78$	$\nu_{1'2'} = 0.25$	$G_{1'2'} = 8.96$
	$E_{2'} = 17.93$	$\nu_{1'3'} = 0.25$	$G_{1'3'} = 8.96$
	$E_{3'} = 17.93$	$\nu_{2'3'} = 0.34$	$G_{2'3'} = 3.45$
Foam	$E = 0.232$	$\nu = 0.20$	$G = \frac{E}{2(1+\nu)}$

Table 3
Definitions of the curvilinear fiber paths for different analysis cases b.

Case	$\phi^{(k=1)} = \phi^{(k=3)}$
b1	15^0
b2	30^0
b3	45^0
b4	60^0

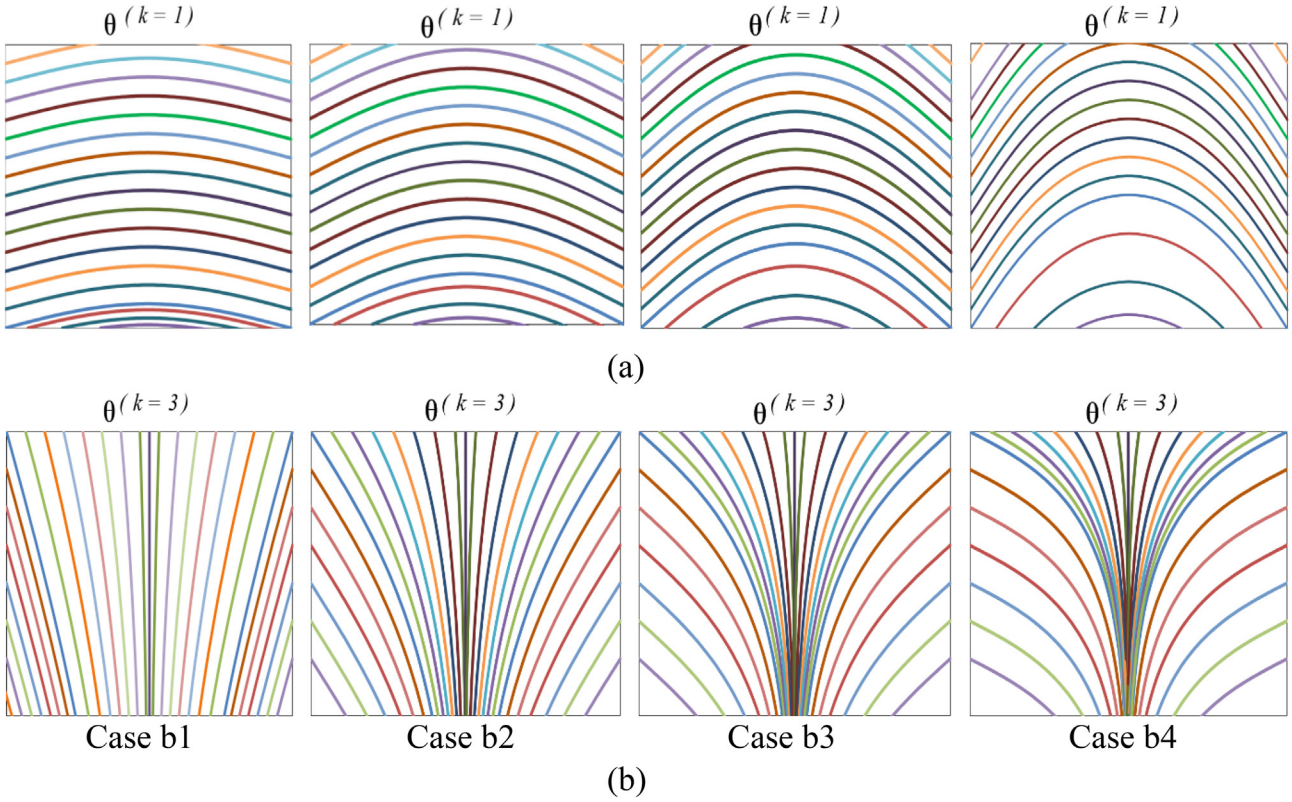

Fig. 11. Various fiber patterns of (a) first and (b) third layers in Case b.

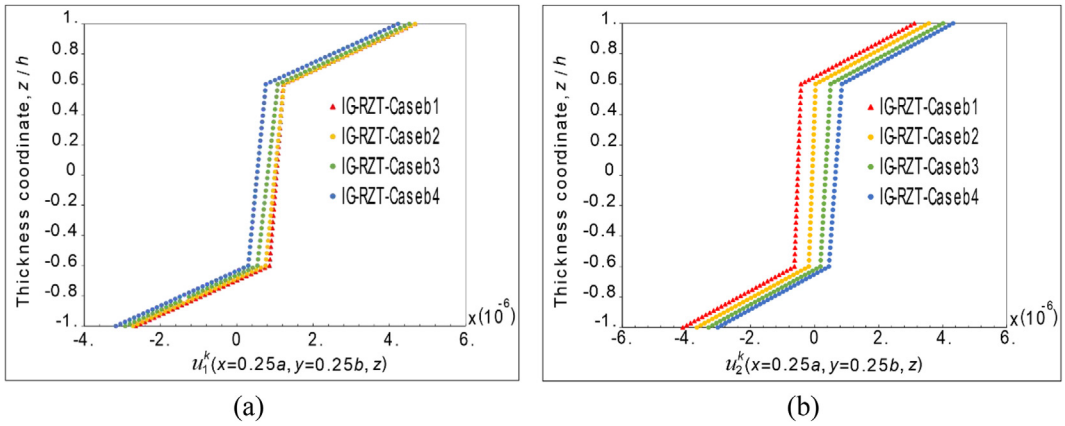

Fig. 12. Zigzag in-plane displacements through the thickness, a)$u_1^{(k)}$ and b) $u_2^{(k)}$(Case b).

imum in-plane displacements through the x-direction, $u_1^{(k)}$, for the first and third layers.

Fig. 13 shows the comparisons of through the thickness in-plane stresses obtained from IG-RZT analysis and the solutions of ANSYS and Tornabene and Bacciochi's approach [45] in which several thickness expansion terms are added into the displacement fields in addition to Murakami's zigzag functions. This ESL approach just as in [47] uses the differential quadrature method to solve the governing equations. The present IG-RZT results have been compared with EDZ4 of [45] which stands for (E)SL-(D)isplacement-Zigzag-Fourth order thickness expansion. For a clear comparison among the established case studies, graphs are divided into two parts: the results for (1) Case b1 and b3, and (2) Case b2 and b4. It is clear from Fig. 13 that the stress results produced by IG-RZT and other solution methods are almost in perfect agreement for all case studies. Thus, the potential capability of IG-RZT formulation is clearly demonstrated for accurately predicting in-plane normal stresses of the sandwich plate possessing any curvilinear path.

It can be deduced from Fig. 14 that the transverse shear stress solutions of IG-RZT and ANSYS have matched perfectly for each four cases. However, the τ_{xz} results of [45] for Case b3 and b4 have a slight discrepancy between IG-RZT and ANSYS. Hence, in the light of these results, the advantages of using IG-RZT formulation for 3-D stress analysis is further validated with respect to a continuum model and shown as compared to reference [45].

5.3. A two-layer circular laminated plate with curvilinear fibers

As a last example, curvilinear fiber laminated circular plate with a radius, $r = 0.5$ $[m]$ and two layers of equal thickness has been analyzed

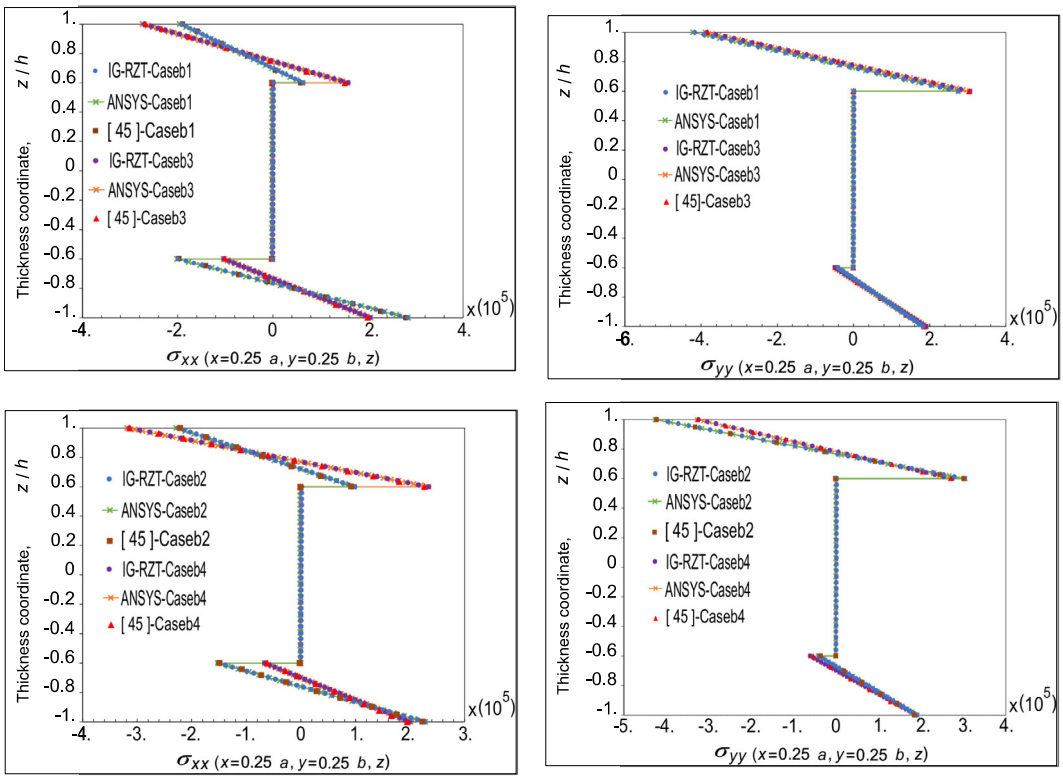

Fig. 13. Comparisons of in-plane stresses, σ_{xx}(left) and σ_{yy}(right) (Case b).

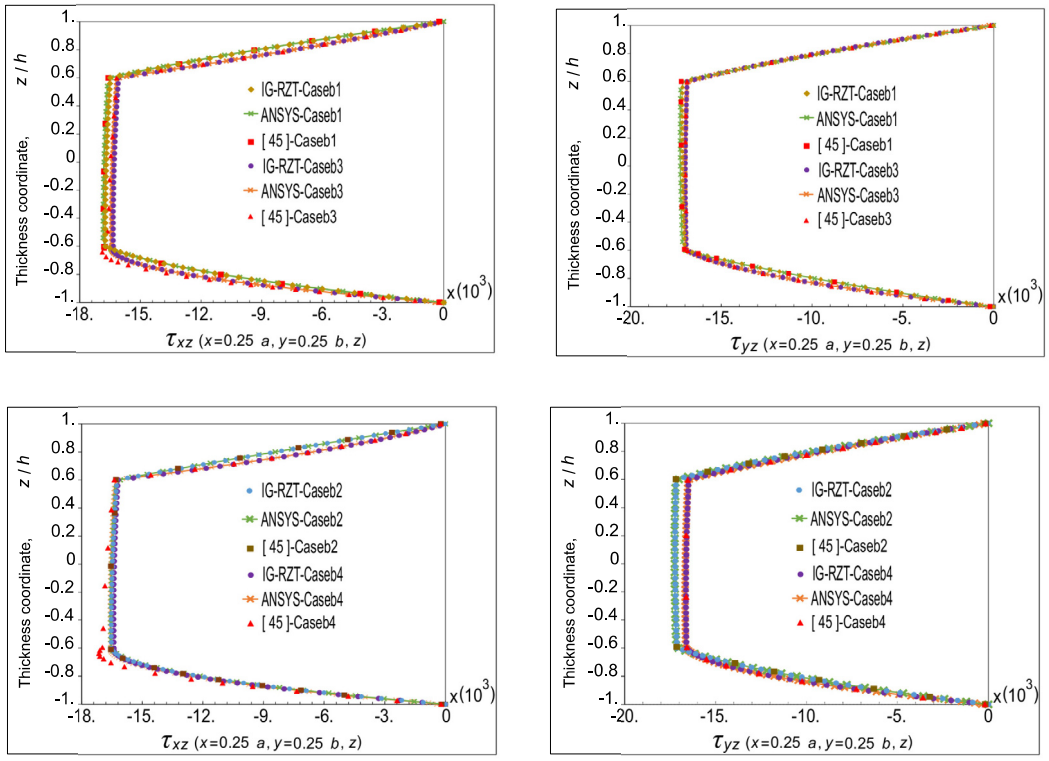

Fig. 14. Comparisons of transverse shear stresses, τ_{xz}(left), τ_{yz}(right) (Case b)

under uniform static loading, $q_z(z=h)=-10\,[kPa]$ with clamped-edge boundary conditions (Case 3). Fig. 15a demonstrates the resulting point, P where the displacement and stress results of the circular plate are obtained. As depicted in Fig. 15b and c, the curvilinear fiber path equations are defined as $y^{(k=1)}=x^2$ and $y^{(k=2)}=x^4$ for the bottom and top layers of the circular plate, respectively. The numerical analy-

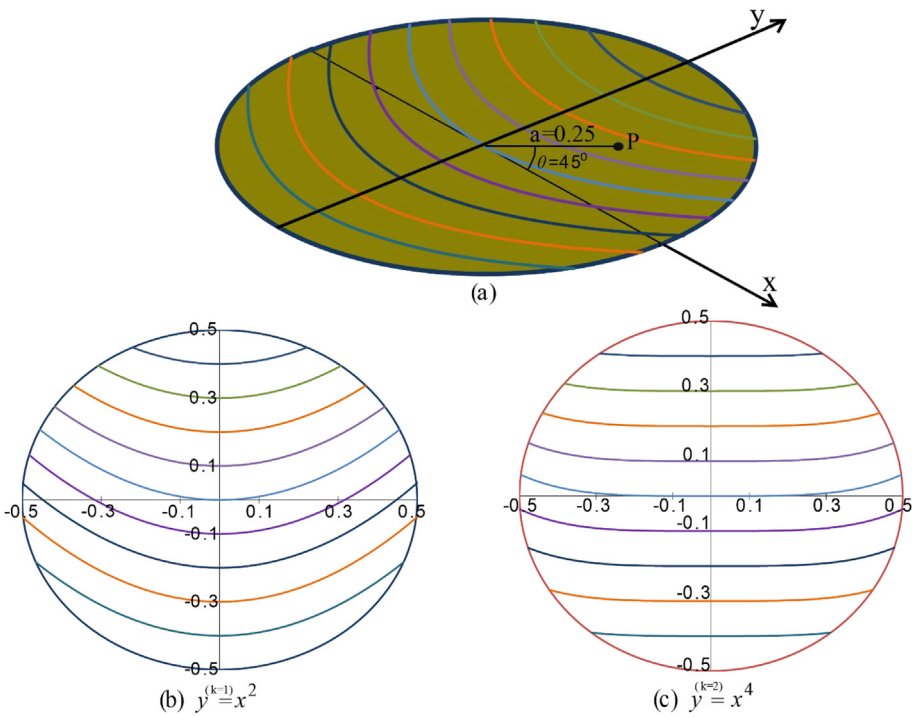

Fig. 15. Curvilinear fiber laminated circular plate (a) with the resulting point P and fiber patterns of (b) bottom and (c) top layers.

ses are performed by considering various span to thickness ratios $(r/2h = 10, 15, 20)$ of the laminate. The displacement and stress results obtained from IG-RZT analysis have been compared with the results of 3-D finite element model generated using Solid 186 element in the commercial ANSYS software. The mechanical properties of the two laminae used in this case are as same as the ones used in Case a of the previous problem (Section 5.1).

The comparisons of in-plane displacements distributions along the thickness coordinate are presented for various span to thickness ratios of the curvilinear fiber laminated circular plate in Fig. 16a and b. As is evident from Fig. 16, no remarkable difference between IG-RZT and ANSYS solutions is observed for in-plane displacement estimations, therefore IG-RZT formulation can capture highly accurate displacement results along the thickness direction of the plate. Moreover, it is important to note that IG-RZT formulation is computationally much efficient than 3-D continuum model (ANSYS-586563 DOF) because IG-RZT (18513 DOF) analysis requires approximately thirty-one times less DOF than those of ANSYS analysis.

Fig. 17a, b and c illustrate the through-the-thickness variation of transverse displacement for various thickness regimes of $r/2h = 10$, 15 and 20, respectively. Classical h-refinement process has been implemented here for IG-RZT with a fixed NURBS degree, $p = 3$. In this regard, it is evident that IG-RZT results obtained by 30×30 mesh correlate very closely with the ANSYS predictions of $40 \times 60 \times 20$ mesh. One can infer from Fig. 17 that the results of IG-RZT become convergent to ANSYS solution despite its low number of DOF for 30×30 discretization. Furthermore, the present IG-RZT formulation can accurately predict the nonlinear variation of the transverse displacements, which can be attributed to the high order thickness coordinate expansion in the kinematic relations. In fact, the potential benefit of using such kinematic relations in the IG-RZT formulation become appealing for the analysis of thick laminates in

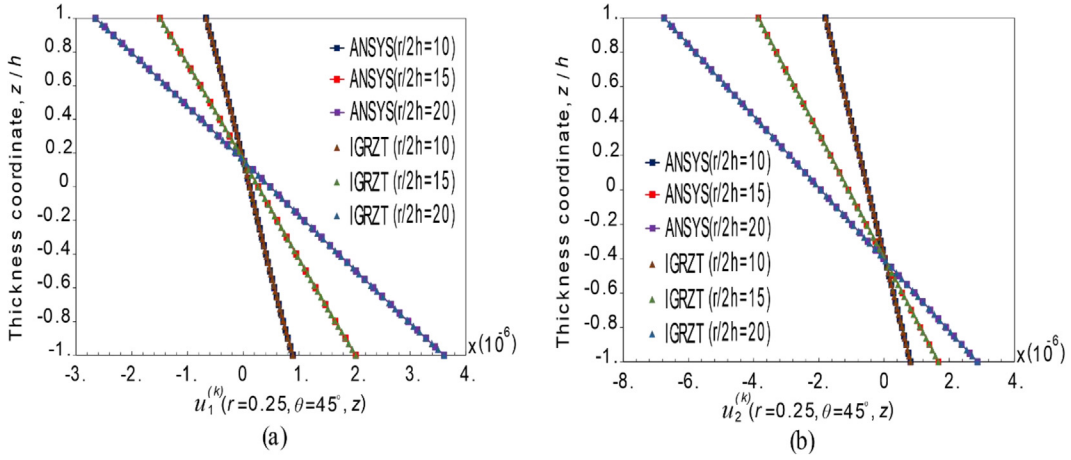

Fig. 16. Through the thickness distributions of in-plane displacements for Case 3

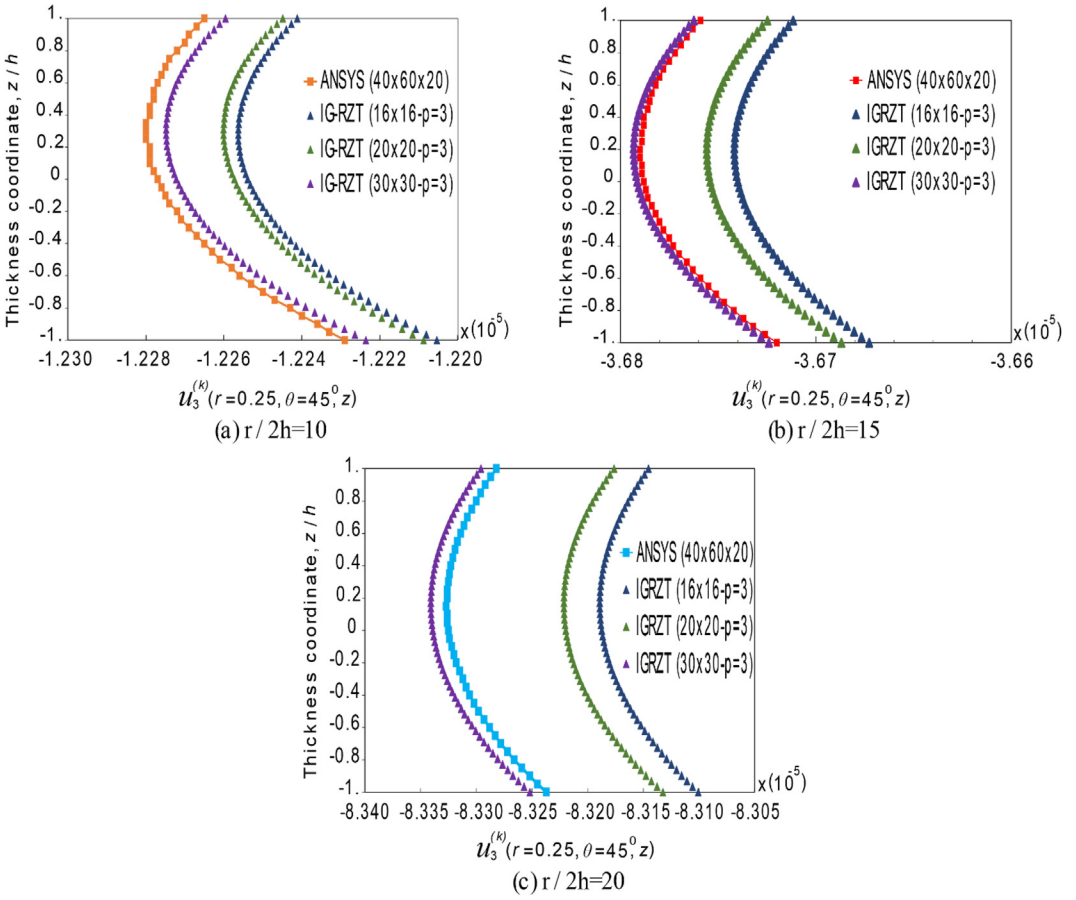

Fig. 17. Comparisons of transverse displacement variation, $u_3^{(k)}$ for Case 3.

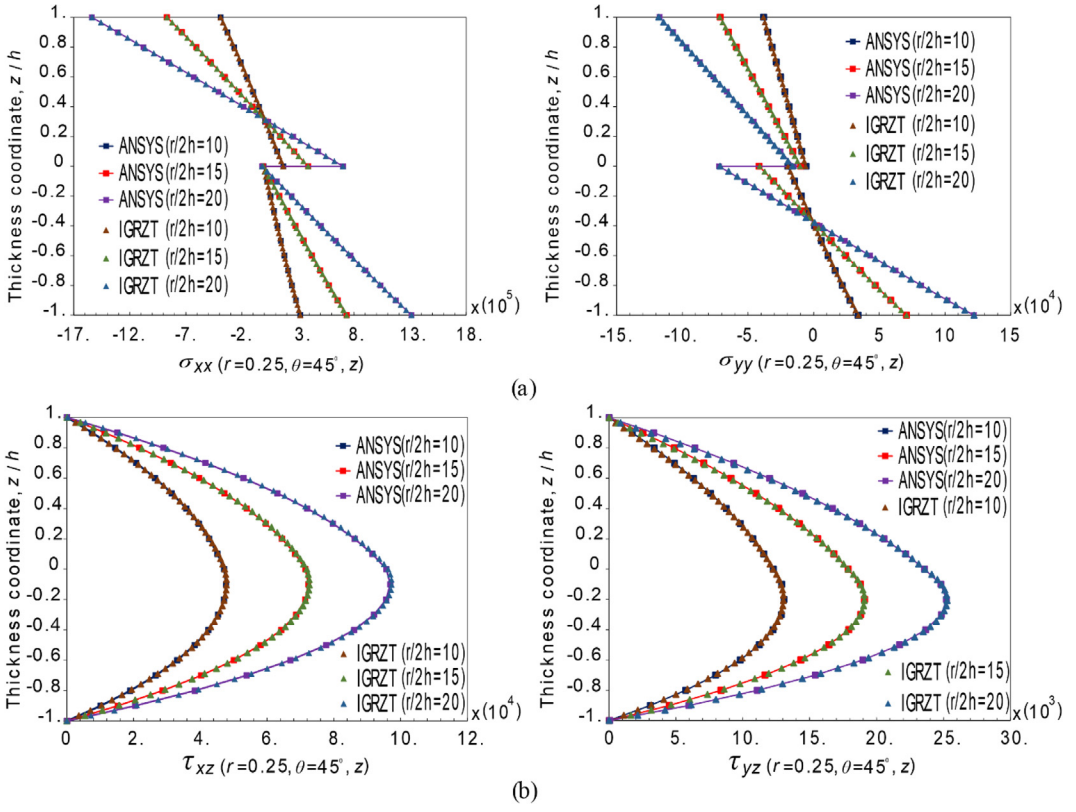

Fig. 18. Comparisons of (a) in-plane stresses and (b) transverse shear stresses for various span to thickness ratios (Case 3).

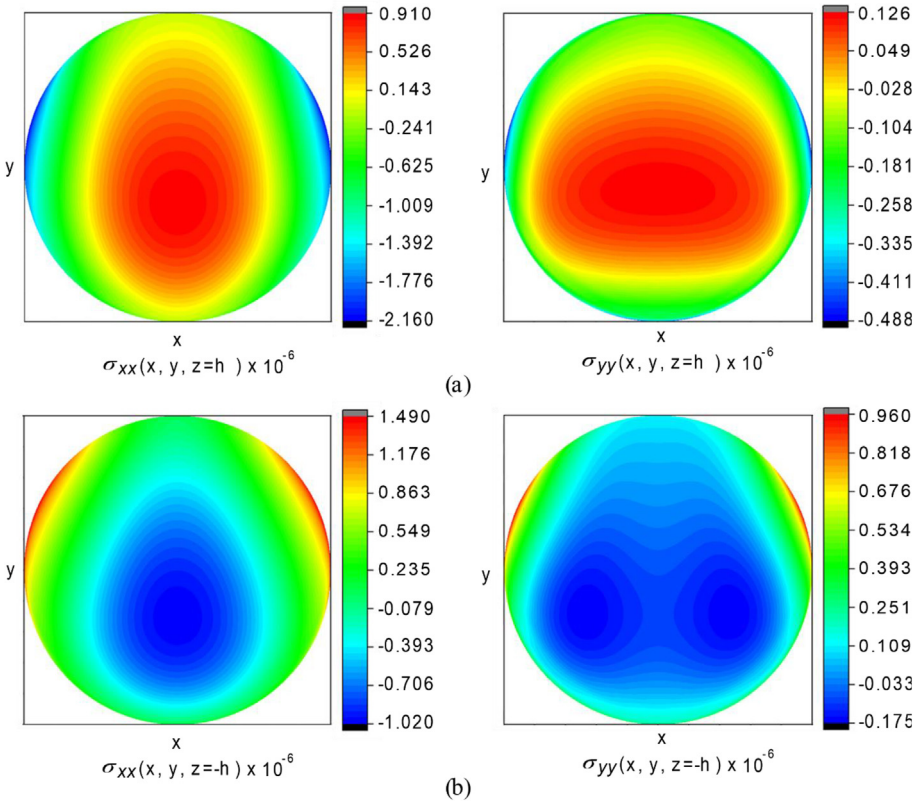

Fig. 19. In-plane normal stress contour plots for (a) top and (b) bottom layers of the circular laminated plate.

Fig. 17a, where the contribution of the thickness stretching effect may not be negligibly small and results in highly nonlinear deflection. Thus, the present IG-RZT formulation can be reliably used for considering these effects in the structural analysis.

The results of Fig. 18a show that IG-RZT is perfectly suited for predicting in-plane normal stresses, σ_{xx}, σ_{yy} in the curvilinear fiber laminated circular plate. In the IG-RZT analysis, a "posteriori" transverse shear stress calculation from the Cauchy's equilibrium equations results in very accurate stress predictions that almost indistinguishably match with 3-D ANSYS model as shown in Fig. 18b. Moreover, we provide the stress contours in Fig. 19 for the clarity of how the in-plane stresses vary at the top and bottom faces of the circular laminated plate. According to all the results presented in this section, the IG-RZT formulation is a general modelling/analysis framework which can be easily utilized to attain highly precise 3-D displacement and stress responses of composite structures manufactured utilizing tailor fiber placement technology.

6. Conclusions

This study presents a novel coupling of isogeometric analysis and RZT formulation for the static analysis of laminated composite structures with curvilinear fibers. Various numerical examples are considered to validate and demonstrate the high accuracy of present IG-RZT mathematical formulation. According to the results generated by IG-RZT and their comparisons with respect to reference solutions, the following observations can be made:

- Linear or quadratic expansion of in-plane displacements with respect to thickness coordinate provides inadequate approximation for VAT composites, thereby leading to erroneous variation of in-plane normal and transverse shear stresses. It is observed that at least a fourth order thickness function should be defined to capture the expected reference stress variation.
- If the thickness stretching contribution is not considered in the definition of out-of-plane displacements, the IG-RZT analysis cannot produce accurate enough displacement/stress results for VAT composites. This fact is still applicable even if high order thickness function is used in the displacement fields.
- According to the comparison between IG-RZT analysis, other methods available in literature and ANSYS 3-D solutions, third order NURBS functions for IG-RZT discretization can estimate convergent displacement/stress results while providing much less DOF as compared to other solutions.
- The kinematic variables of RZT are independent of the number of layers which reduce computational effort especially in the analysis of thick laminates. RZT does not enforce the continuity of the transverse shear stresses at the layer interfaces, and thus the shear stresses from the constitutive equations are obtained as average piecewise constant values at the laminae. However, the results can be much improved by the computation of τ_{xz}, τ_{yz} stresses from "a posteriori" process where the axial stress fields and C^2 NURBS shape functions are used in Cauchy's equilibrium equations. According to this post-processing, it is demonstrated that the IG-RZT methodology can be suitably utilized for accurate predictions of the transverse shear stresses in VAT composites.

Overall, these concluding remarks mainly confirm the robustness, high accuracy, and potential applicability of IG-RZT formulation for comprehensive modelling and analysis of multi-layered composite and sandwich structures with curvilinear fibers. We believe that the IG-RZT methodology can be a computationally very efficient and profound candidate for performing the optimization of the laminated plates with curvilinear fibers which can be subject of a further investigation in the future studies.

7. Authors' contributions

Kazim Ahmet Hasim and Adnan Kefal have developed the formulation together. Kazim Ahmet Hasim has implemented the formulation and obtained the numerical results using Mathematica and ANSYS. Kazim Ahmet Hasim and Adnan Kefal have written the paper together.

CRediT authorship contribution statement

K.A. Hasim: Conceptualization, Methodology, Software, Validation, Writing - original draft, Writing - review & editing. **A. Kefal:** Conceptualization, Methodology, Writing - original draft, Writing - review & editing.

Declaration of Competing Interest

The authors declare that they have no known competing financial interests or personal relationships that could have appeared to influence the work reported in this paper.

Acknowledgements

None. This research did not receive any specific grant from funding agencies in the public, commercial, or not-for-profit sectors.

Appendix A

The standard Hooke stress–strain relationship for the k-th orthotropic layer defined in Eq. (10) can be written explicitly as:

$$\begin{bmatrix}\sigma_x\\ \sigma_y\\ \sigma_z\\ \tau_{xz}\\ \tau_{yz}\\ \tau_{xy}\end{bmatrix}^{(k)} = \begin{bmatrix}\bar{Q}_{11} & \bar{Q}_{12} & \bar{Q}_{13} & 0 & 0 & \bar{Q}_{16}\\ \bar{Q}_{12} & \bar{Q}_{22} & \bar{Q}_{23} & 0 & 0 & \bar{Q}_{26}\\ \bar{Q}_{13} & \bar{Q}_{23} & \bar{Q}_{33} & 0 & 0 & \bar{Q}_{36}\\ 0 & 0 & 0 & \bar{Q}_{44} & \bar{Q}_{45} & 0\\ 0 & 0 & 0 & \bar{Q}_{45} & \bar{Q}_{55} & 0\\ \bar{Q}_{16} & \bar{Q}_{26} & \bar{Q}_{36} & 0 & 0 & \bar{Q}_{66}\end{bmatrix}^{(k)} \begin{bmatrix}\varepsilon_x\\ \varepsilon_y\\ \varepsilon_z\\ \gamma_{xz}\\ \gamma_{yz}\\ \gamma_{xy}\end{bmatrix}^{(k)} = \boldsymbol{D}^{(k)}\boldsymbol{\varepsilon}^{(k)} \tag{A1}$$

The constitutive matrix in Eq. (A1), $\boldsymbol{D}^{(k)}$ can be obtained by the transformation of natural coordinate system (1,2,3) to the laminate coordinate system (x,y,z). It can be expressed as:

$$\boldsymbol{D}^{(k)} = \left(\boldsymbol{T}^{(k)}\right)^{T}\tilde{\boldsymbol{D}}^{(k)}\boldsymbol{T}^{(k)} \tag{A2}$$

with

$$\boldsymbol{T}^{(k)} = \begin{bmatrix} c^2 & s^2 & 0 & 0 & 0 & -2sc\\ s^2 & c^2 & 0 & 0 & 0 & 2sc\\ 0 & 0 & 1 & 0 & 0 & 0\\ 0 & 0 & 0 & c & -s & 0\\ 0 & 0 & 0 & s & c & 0\\ sc & -sc & 0 & 0 & 0 & c^2-s^2\end{bmatrix} \tag{A3a}$$

and

$$\tilde{\boldsymbol{D}}^{(k)} = \begin{bmatrix} Q_{11} & Q_{12} & Q_{13} & 0 & 0 & 0\\ Q_{12} & Q_{22} & Q_{23} & 0 & 0 & 0\\ Q_{13} & Q_{23} & Q_{33} & 0 & 0 & 0\\ 0 & 0 & 0 & G_{13} & 0 & 0\\ 0 & 0 & 0 & 0 & G_{23} & 0\\ 0 & 0 & 0 & 0 & 0 & G_{12}\end{bmatrix}^{(k)} \tag{A3b}$$

where $c = \cos\theta^{(k)}$ and $s = \sin\theta^{(k)}$ with $\theta^{(k)}$ denoting the angle between the fiber longitudinal (1) and global x axes. The coefficients of this constitutive matrix, $\tilde{\boldsymbol{D}}^{(k)}$ are related to the longitudinal (1) and transverse (2,3) elasticity and shear moduli, $E_i^{(k)}$, $\nu_{ij}^{(k)}$ and $G_{ij}^{(k)}$ by

$$Q_{11}^{(k)} = E_1^{(k)}\frac{1-\nu_{23}^{(k)}\nu_{32}^{(k)}}{\Delta^{(k)}} \tag{A4a}$$

$$Q_{12}^{(k)} = E_1^{(k)}\frac{\nu_{21}^{(k)}+\nu_{31}^{(k)}\nu_{23}^{(k)}}{\Delta^{(k)}} \tag{A4b}$$

$$Q_{13}^{(k)} = E_3^{(k)}\frac{\nu_{13}^{(k)}+\nu_{12}^{(k)}\nu_{23}^{(k)}}{\Delta^{(k)}} \tag{A4c}$$

$$Q_{22}^{(k)} = E_2^{(k)}\frac{1-\nu_{13}^{(k)}\nu_{31}^{(k)}}{\Delta^{(k)}} \tag{A4d}$$

$$Q_{23}^{(k)} = E_3^{(k)}\frac{\nu_{23}^{(k)}+\nu_{21}^{(k)}\nu_{13}^{(k)}}{\Delta^{(k)}} \tag{A4e}$$

$$Q_{33}^{(k)} = E_3^{(k)}\frac{1-\nu_{12}^{(k)}\nu_{21}^{(k)}}{\Delta^{(k)}} \tag{A4f}$$

$$\Delta^{(k)} = 1-\nu_{12}^{(k)}\nu_{21}^{(k)}-\nu_{23}^{(k)}\nu_{32}^{(k)}-\nu_{31}^{(k)}\nu_{13}^{(k)}-2\nu_{21}^{(k)}\nu_{32}^{(k)}\nu_{13}^{(k)} \tag{A4g}$$

Appendix B

The matrices, $\boldsymbol{B}_I^{\alpha}$, $(\alpha = 1,2,\ldots,6)$ used in Eq. (19b) contains NURBS functions with the derivatives and can be expressed as:

$$\boldsymbol{B}_I^{1} = \begin{bmatrix} R_{I,x} & 0 & 0 & 0 & 0 & 0 & 0&0&0&0&0&0&0&0&0&0\\ 0 & R_{I,x} & 0 & 0 & 0 & 0 & 0&0&0&0&0&0&0&0&0&0\\ 0 & 0 & R_{I,x} & 0 & 0 & 0 & 0&0&0&0&0&0&0&0&0&0\\ 0 & 0 & 0 & R_{I,x} & 0 & 0 & 0&0&0&0&0&0&0&0&0&0\\ 0 & 0 & 0 & 0 & R_{I,x} & 0 & 0&0&0&0&0&0&0&0&0&0\\ 0 & 0 & 0 & 0 & 0 & R_{I,x} & 0&0&0&0&0&0&0&0&0&0\\ 0 & 0 & 0 & 0 & 0 & R_I & 0&0&0&0&0&0&0&0&0&0\end{bmatrix}_{7\times 17} \tag{B1a}$$

$$\boldsymbol{B}_I^{2} = \begin{bmatrix} 0&0&0&0&0&0&R_{I,y}&0&0&0&0&0&0&0&0&0\\ 0&0&0&0&0&0&0&R_{I,y}&0&0&0&0&0&0&0&0\\ 0&0&0&0&0&0&0&0&R_{I,y}&0&0&0&0&0&0&0\\ 0&0&0&0&0&0&0&0&0&R_{I,y}&0&0&0&0&0&0\\ 0&0&0&0&0&0&0&0&0&0&R_{I,y}&0&0&0&0&0\\ 0&0&0&0&0&0&0&0&0&0&0&R_{I,y}&0&0&0&0\\ 0&0&0&0&0&0&0&0&0&0&0&R_I&0&0&0&0\end{bmatrix}_{7\times 17} \tag{B1b}$$

$$\boldsymbol{B}_I^{3} = \begin{bmatrix} 0&0&0&0&0&0&0&0&0&0&0&0&0&R_I&0&0&0\\ 0&0&0&0&0&0&0&0&0&0&0&0&0&0&R_I&0&0\\ 0&0&0&0&0&0&0&0&0&0&0&0&0&0&0&R_I&0\\ 0&0&0&0&0&0&0&0&0&0&0&0&0&0&0&0&R_I\end{bmatrix}_{4\times 17} \tag{B1c}$$

$$\boldsymbol{B}_I^{4} = \begin{bmatrix} 0&R_I&0&0&0&0&0&0&0&0&0&0&0&0&0&0&0\\ 0&0&R_I&0&0&0&0&0&0&0&0&0&0&0&0&0&0\\ 0&0&0&R_I&0&0&0&0&0&0&0&0&0&0&0&0&0\\ 0&0&0&0&R_I&0&0&0&0&0&0&0&0&0&0&0&0\\ 0&0&0&0&0&R_I&0&0&0&0&0&0&0&0&0&0&0\\ 0&0&0&0&0&0&0&0&0&0&0&0&R_{I,x}&0&0&0&0\\ 0&0&0&0&0&0&0&0&0&0&0&0&0&R_{I,x}&0&0&0\\ 0&0&0&0&0&0&0&0&0&0&0&0&0&0&R_{I,x}&0&0\\ 0&0&0&0&0&0&0&0&0&0&0&0&0&0&0&R_{I,x}&0\\ 0&0&0&0&0&0&0&0&0&0&0&0&0&0&0&0&R_{I,x}\end{bmatrix}_{10\times 17} \tag{B1d}$$

$$\boldsymbol{B}_I^{5} = \begin{bmatrix} 0&0&0&0&0&0&0&R_I&0&0&0&0&0&0&0&0&0\\ 0&0&0&0&0&0&0&0&R_I&0&0&0&0&0&0&0&0\\ 0&0&0&0&0&0&0&0&0&R_I&0&0&0&0&0&0&0\\ 0&0&0&0&0&0&0&0&0&0&R_I&0&0&0&0&0&0\\ 0&0&0&0&0&0&0&0&0&0&0&R_I&0&0&0&0&0\\ 0&0&0&0&0&0&0&0&0&0&0&0&R_{I,y}&0&0&0&0\\ 0&0&0&0&0&0&0&0&0&0&0&0&0&R_{I,y}&0&0&0\\ 0&0&0&0&0&0&0&0&0&0&0&0&0&0&R_{I,y}&0&0\\ 0&0&0&0&0&0&0&0&0&0&0&0&0&0&0&R_{I,y}&0\\ 0&0&0&0&0&0&0&0&0&0&0&0&0&0&0&0&R_{I,y}\end{bmatrix}_{10\times 17} \tag{B1e}$$

$$\boldsymbol{B}_I^6 = \begin{bmatrix} R_{I,y} & 0 & 0 & 0 & 0 & 0 & 0 & 0 & 0 & 0 & 0 & 0 & 0 & 0 & 0 & 0 & 0 \\ 0 & R_{I,y} & 0 & 0 & 0 & 0 & 0 & 0 & 0 & 0 & 0 & 0 & 0 & 0 & 0 & 0 & 0 \\ 0 & 0 & R_{I,y} & 0 & 0 & 0 & 0 & 0 & 0 & 0 & 0 & 0 & 0 & 0 & 0 & 0 & 0 \\ 0 & 0 & 0 & R_{I,y} & 0 & 0 & 0 & 0 & 0 & 0 & 0 & 0 & 0 & 0 & 0 & 0 & 0 \\ 0 & 0 & 0 & 0 & R_{I,y} & 0 & 0 & 0 & 0 & 0 & 0 & 0 & 0 & 0 & 0 & 0 & 0 \\ 0 & 0 & 0 & 0 & 0 & R_{I,y} & 0 & 0 & 0 & 0 & 0 & 0 & 0 & 0 & 0 & 0 & 0 \\ 0 & 0 & 0 & 0 & 0 & R_I & 0 & 0 & 0 & 0 & 0 & 0 & 0 & 0 & 0 & 0 & 0 \\ 0 & 0 & 0 & 0 & 0 & 0 & R_{I,x} & 0 & 0 & 0 & 0 & 0 & 0 & 0 & 0 & 0 & 0 \\ 0 & 0 & 0 & 0 & 0 & 0 & 0 & R_{I,x} & 0 & 0 & 0 & 0 & 0 & 0 & 0 & 0 & 0 \\ 0 & 0 & 0 & 0 & 0 & 0 & 0 & 0 & R_{I,x} & 0 & 0 & 0 & 0 & 0 & 0 & 0 & 0 \\ 0 & 0 & 0 & 0 & 0 & 0 & 0 & 0 & 0 & R_{I,x} & 0 & 0 & 0 & 0 & 0 & 0 & 0 \\ 0 & 0 & 0 & 0 & 0 & 0 & 0 & 0 & 0 & 0 & R_{I,x} & 0 & 0 & 0 & 0 & 0 & 0 \\ 0 & 0 & 0 & 0 & 0 & 0 & 0 & 0 & 0 & 0 & 0 & R_{I,x} & 0 & 0 & 0 & 0 & 0 \\ 0 & 0 & 0 & 0 & 0 & 0 & 0 & 0 & 0 & 0 & 0 & R_I & 0 & 0 & 0 & 0 & 0 \end{bmatrix}_{14 \times 17} \tag{B1f}$$

References

[1] Toledano A, Murakami H. A composite plate theory for arbitrary laminate configurations. J Appl Mech Trans ASME 1987;54:181–9. https://doi.org/10.1115/1.3172955.

[2] Ferreira AJM, Fasshauer GE, Batra RC, Rodrigues JD. Static deformations and vibration analysis of composite and sandwich plates using a layerwise theory and RBF-PS discretizations with optimal shape parameter. Compos Struct 2008;86:328–43. https://doi.org/10.1016/j.compstruct.2008.07.025.

[3] Thai CH, Ferreira AJM, Carrera E, Nguyen-Xuan H. Isogeometric analysis of laminated composite and sandwich plates using a layerwise deformation theory. Compos Struct 2013;104:196–214. https://doi.org/10.1016/j.compstruct.2013.04.002.

[4] Carrera E. Evaluation of layerwise mixed theories for laminated plates analysis. AIAA J 1998;36:830–9. https://doi.org/10.2514/2.444.

[5] Ferreira AJM. Analysis of composite plates using a layerwise theory and multiquadrics discretization. Mech Adv Mater Struct 2005;12:99–112. https://doi.org/10.1080/15376490490493952.

[6] Thai CH, Ferreira AJM, Abdel Wahab M, Nguyen-Xuan H. A generalized layerwise higher-order shear deformation theory for laminated composite and sandwich plates based on isogeometric analysis. Acta Mech 2016;227:1225–50. https://doi.org/10.1007/s00707-015-1547-4.

[7] Barut A, Madenci E, Anderson T, Tessler A. Equivalent single-layer theory for a complete stress field in sandwich panels under arbitrarily distributed loading. Compos Struct 2002;58(4):483–95. https://doi.org/10.1016/S0263-8223(02)00137-X.

[8] Abrate S, Di Sciuva M. Equivalent single layer theories for composite and sandwich structures: a review. Compos Struct 2017;179:482–94. https://doi.org/10.1016/j.compstruct.2017.07.090.

[9] Loredo A, D'Ottavio M, Vidal P, Polit O. A family of higher-order single layer plate models meeting Cz0-requirements for arbitrary laminates. Compos Struct 2019;225:. https://doi.org/10.1016/j.compstruct.2019.111146111146.

[10] Rao KM, Meyer-Piening HR. Analysis of thick laminated anisotropic composite plates by the finite element method. Compos Struct 1990;15:185–213. https://doi.org/10.1016/0263-8223(90)90031-9.

[11] Murakami H. Laminated composite plate theory with improved in-plane responses. J Appl Mech Trans ASME 1986;53:661–6. https://doi.org/10.1115/1.3171828.

[12] Tessler AM di S. In: Refinement of Timoshenko Beam Theory for Composite and Sandwich Beams Using Zigzag Kinematics. NASA/TP-2007-215086, Natl Aeronaut Sp Adm. p. 45.

[13] Tessler A, Di Sciuva M, Gherlone M. A refined zigzag beam theory for composite and sandwich beams. J Compos Mater 2009;43:1051–81. https://doi.org/10.1177/0021998308097730.

[14] Tessler A, Di Sciuva M, Gherlone M. Refined zigzag theory for homogeneous, laminated composite, and sandwich plates: A Homogeneous Limit Methodology for Zigzag Function Selection. NASA/TP-2010-216214, Natl Aeronaut Sp Adm, 2010.

[15] Tessler A, Gherlone M, Versino D, Di Sciuva M. In: Analytic and computational perspectives of multi-scale theory for homogeneous. Laminated composite, and sandwich beams and plates. NASA/TP-2012-217573, Natl Aeronaut Sp Adm. https://doi.org/10.1541/ieejpes.140.nl1_1.

[16] Averill RC. Static and dynamic response of moderately thick laminated beams with damage. Compos Eng 1994;4:381–95. https://doi.org/10.1016/s0961-9526(09)80013-0.

[17] Averill RC, Yip YC. Development of simple, robust finite elements based on refined theories for thick laminated beams. Comput Struct 1996;59(3):529–46. https://doi.org/10.1111/j.1540-8159.2011.03079.x.

[18] Aitharaju VR, Averill RC. An assessment of zig-zag kinematic displacement models for the analysis of laminated composites. Mech Compos Mat Struct 1999;6:1–26.

[19] Gherlone M. On the use of zigzag functions in equivalent single layer theories for laminated composite and sandwich beams: a comparative study and some observations on external weak layers. J Appl Mech Trans ASME 2013;80:1–20. https://doi.org/10.1115/1.4023690.

[20] Iurlaro L, Gherlone M, Sciuva M Di, Tessler A. Assessment of the Refined Zigzag Theory for bending, vibration, and buckling of sandwich plates : a comparative study of different theories. Compos Struct 2013;106:777–92. https://doi.org/10.1016/j.compstruct.2013.07.019.

[21] Barut A, Madenci E, Tessler A. C 0-continuous triangular plate element for laminated composite and sandwich plates using the 2, 2 – Refined Zigzag Theory. Compos Struct 2013;106:835–53. https://doi.org/10.1016/j.compstruct.2013.07.024.

[22] Hasim KA. Isogeometric static analysis of laminated composite plane beams by using refined zigzag theory. Compos Struct 2018;186:365–74. https://doi.org/10.1016/j.compstruct.2017.12.033.

[23] Hasim KA, Kefal A, Madenci E. Isogeometric plate element for unstiffened and blade stiffened laminates based on refined zigzag theory. Compos Struct 2019;222:. https://doi.org/10.1016/j.compstruct.2019.110931110931.

[24] Kefal A, Hasim KA, Yildiz M. A novel isogeometric beam element based on mixed form of refined zigzag theory for thick sandwich and multilayered composite beams. Compos Part B Eng 2019;167:100–21. https://doi.org/10.1016/j.compositesb.2018.11.102.

[25] Versino D, Gherlone M, Mattone M, Di Sciuva M, Tessler A. C0 triangular elements based on the Refined Zigzag Theory for multilayer composite and sandwich plates. Compos Part B Eng 2013;44:218–30. https://doi.org/10.1016/j.compositesb.2012.05.026.

[26] Ascione A, Gherlone M. Nonlinear static response analysis of sandwich beams using the Refined Zigzag Theory. J Sandw Struct Mater 2018. https://doi.org/10.1177/1099636218795381.

[27] Leissa AW, Martin AF. Vibration and buckling of rectangular composite plates with variable fiber spacing. Compos Struct 1990;14:339–57. https://doi.org/10.1016/0263-8223(90)90014-6.

[28] Dinardo MT, Lagacet PA. Buckling and Postbuckling of Laminated Composite Plates with Ply Dropoffs. AIAA J 1989;27:1392–8.

[29] Abdalla MM, Setoodeh S, Gürdal Z. Design of variable stiffness composite panels for maximum fundamental frequency using lamination parameters. Compos Struct 2007;81:283–91. https://doi.org/10.1016/j.compstruct.2006.08.018.

[30] Hyer MW, Lee HH. The use of curvilinear fiber format to improve buckling resistance of composite plates with central circular holes. Compos Struct 1991;18:239–61.

[31] Tosh MW, Kelly DW. On the design, manufacture and testing of trajectorial fibre steering for carbon fibre composite laminates. Compos Part A: Appl Sci Manuf 2000;31:1047–60.

[32] Hyer M, Rust R, Waters. Innovative design of composite structures: Design, manufacturing, and testing of plates utilizing curvilinear fiber trajectories; 1994.

[33] Tatting BF, Gürdal Z. Design and manufacture tow placed plates of elastically tailored. NASA/CR-2002-211919, Natl Aeronaut Sp Adm, 2002.

[34] Raspall F, Velu R, Vaheed NM. Fabrication of complex 3D composites by fusing automated fiber placement (AFP) and additive manufacturing (AM) technologies. Adv Manuf Polym Compos Sci 2019;5:6–16. https://doi.org/10.1080/20550340.2018.1557397.

[35] Bullock F, Kowalski S, Young R. Automated prepreg tow placement for composite structures. Adv Mater Chall NEXT Decad 1990;1:734–45.

[36] Le-Manh T, Lee J. Stacking sequence optimization for maximum strengths of laminated composite plates using genetic algorithm and isogeometric analysis. Compos Struct 2014;116:357–63. https://doi.org/10.1016/j.compstruct.2014.05.011.

[37] Soremekun G, Gürdal Z, Haftka RT, Watson LT. Composite laminate design optimization by genetic algorithm with generalized elitist selection. Comput Struct 2001;79:131–43. https://doi.org/10.1016/S0045-7949(00)00125-5.

[38] Setoodeh S, Abdalla MM, IJsselmuiden ST, Gürdal Z. Design of variable-stiffness composite panels for maximum buckling load. Compos Struct 2009;87:109–17. https://doi.org/10.1016/j.compstruct.2008.01.008.
[39] Setoodeh S, Abdalla MM, Gürdal Z. Design of variable-stiffness laminates using lamination parameters. Compos Part B Eng 2006;37:301–9. https://doi.org/10.1016/j.compositesb.2005.12.001.
[40] Akbarzadeh AH, Arian Nik M, Pasini D. The role of shear deformation in laminated plates with curvilinear fiber paths and embedded defects. Compos Struct 2014;118:217–27. https://doi.org/10.1016/j.compstruct.2014.07.027.
[41] Yazdani S, Ribeiro P. Geometrically non-linear static analysis of unsymmetric composite plates with curvilinear fibres: p-version layerwise approach. Compos Struct 2014;118:74–85. https://doi.org/10.1016/j.compstruct.2014.07.007.
[42] Venkatachari A, Natarajan S, Ramajeyathilagam K, Ganapathi M. Assessment of certain higher-order structural models based on global approach for bending analysis of curvilinear composite laminates. Compos Struct 2014;118:548–59. https://doi.org/10.1016/j.compstruct.2014.07.045.
[43] Viglietti A, Zappino E, Carrera E. Analysis of variable angle tow composites structures using variable kinematic models. Compos Part B 2019;171:272–83. https://doi.org/10.1016/j.compositesb.2019.03.072.
[44] Demasi L, Biagini G, Vannucci F, Santarpia E, Cavallaro R. Equivalent Single Layer, Zig-Zag, and Layer Wise theories for variable angle tow composites based on the Generalized Unified Formulation. Compos Struct 2017;177:54–79. https://doi.org/10.1016/j.compstruct.2017.06.033.
[45] Tornabene F, Bacciocchi M. Effect of curvilinear reinforcing fibers on the linear static behavior of soft-core sandwich structures. J Compos Sci 2018;2:14. https://doi.org/10.3390/jcs2010014.
[46] Groh RMJ, Weaver PM, White S, Raju G, Wu Z. A 2D equivalent single-layer formulation for the effect of transverse shear on laminated plates with curvilinear fibres Classical Theory of Plates. Compos Struct 2013;100:464–78. https://doi.org/10.1016/j.compstruct.2013.01.014.
[47] Tornabene F, Fantuzzi N, Bacciocchi M. Higher-order structural theories for the static analysis of doubly-curved laminated composite panels reinforced by curvilinear fibers. Thin Walled Struct 2016;102:222–45. https://doi.org/10.1016/j.tws.2016.01.029.
[48] Piegl L, Tiller W. The NURBS Book; 1996. https://doi.org/10.1016/0010-4485(96)86819-9.
[49] Hughes TJR, Cottrell JA, Bazilevs Y. Isogeometric analysis: CAD, finite elements, NURBS, exact geometry and mesh refinement. Comput Methods Appl Mech Eng 2005;194:4135–95. https://doi.org/10.1016/j.cma.2004.10.008.
[50] Cottrell JA, Hughes TJR, Bazilevs Y. Isogeometric analysis toward integration of CAD and FEA. United Kingdom: John Wley & Sons Ltd.; 2009.
[51] Liu N, Jeffers AE. Isogeometric analysis of laminated composite and functionally graded sandwich plates based on a layerwise displacement theory. Compos Struct 2017;176:143–53. https://doi.org/10.1016/j.compstruct.2017.05.037.
[52] Thai CH, Kulasegaram S, Tran LV, Nguyen-Xuan H. Generalized shear deformation theory for functionally graded isotropic and sandwich plates based on isogeometric approach. Comput Struct 2014;141:94–112. https://doi.org/10.1016/j.compstruc.2014.04.003.
[53] Nguyen TN, Thai CH, Luu A-T, Nguyen-Xuan H, Lee J. NURBS-based postbuckling analysis of functionally graded carbon nanotube-reinforced composite shells. Comput Methods Appl Mech Eng 2019;347:983–1003. https://doi.org/10.1016/j.cma.2019.01.011.
[54] Shi P, Dong C, Sun F, Liu W, Hu Q. A new higher order shear deformation theory for static, vibration and buckling responses of laminated plates with the isogeometric analysis. Compos Struct 2018;204:342–58. https://doi.org/10.1016/j.compstruct.2018.07.080.
[55] Nguyen TN, Ngo TD, Nguyen-Xuan H. A novel three-variable shear deformation plate formulation: Theory and Isogeometric implementation. Comput Methods Appl Mech Eng 2017;326:376–401. https://doi.org/10.1016/j.cma.2017.07.024.
[56] Nguyen QH, Nguyen LB, Nguyen HB, Nguyen-Xuan H. A three-variable high order shear deformation theory for isogeometric free vibration, buckling and instability analysis of FG porous plates reinforced by graphene platelets. Compos Struct 2020;245:. https://doi.org/10.1016/j.compstruct.2020.112321112321.
[57] Fantuzzi N, Tornabene F. Strong Formulation Isogeometric Analysis (SFIGA) for laminated composite arbitrarily shaped plates. Compos Part B Eng 2016;96:173–203. https://doi.org/10.1016/j.compositesb.2016.04.034.
[58] Thanh C-L, Ferreira AJM, Abdel Wahab M. A refined size-dependent couple stress theory for laminated composite micro-plates using isogeometric analysis. Thin-Walled Struct 2019;145:. https://doi.org/10.1016/j.tws.2019.106427106427.
[59] Thanh C-L, Tran LV, Vu-Huu T, Abdel-Wahab M. The size-dependent thermal bending and buckling analyses of composite laminate microplate based on new modified couple stress theory and isogeometric analysis. Comput Methods Appl Mech Eng 2019;350:337–61. https://doi.org/10.1016/j.cma.2019.02.028.
[60] Tessler A, Di Sciuva M, Gherlone M. A consistent refinement of first-order shear deformation theory for laminated composite and sandwich plates using improved zigzag kinematics. J Mech Mater Struct 2010;5:341–67. https://doi.org/10.2140/jomms.2010.5.341.
[61] Koiter WT. A consistent first approximation in the general theory of thin elastic shells. Delft: Laboratorium voor Toegepaste Mechanica der Technische Hogeschool; 1959.
[62] Carrera E, Brischetto S, Cinefra M, Soave M. Effects of thickness stretching in functionally graded plates and shells. Compos Part B Eng 2011;42:123–33. https://doi.org/10.1016/j.compositesb.2010.10.005.